WAPD-TM-1304
DOE RESEARCH AND
DEVELOPMENT REPORT

A MODEL TO PREDICT SWELLING, GAS RELEASE, AND DENSIFICATION IN OXIDE FUELS

(AWBA Development Program)

JUNE 1978

CONTRACT EY-76-C-11-0014

BETTIS ATOMIC POWER LABORATORY
WEST MIFFLIN, PENNSYLVANIA

Operated for the U. S. Department of Energy by

WESTINGHOUSE ELECTRIC CORPORATION

DISCLAIMER

WAPD-TM-1304
Special External Distribution

A MODEL TO PREDICT SWELLING, GAS RELEASE, AND DENSIFICATION IN OXIDE FUELS
(AWBA Development Program)

C. C. Dollins

June 1978

Contract EY-76-C-11-0014

Printed in the United States of America
Available from the
National Technical Information Service
U. S. Department of Commerce
5285 Port Royal Road
Springfield, Virginia 22151

NOTE

This document is an interim memorandum prepared primarily for internal reference and does not represent a final expression of the opinion of Westinghouse. When this memorandum is distributed externally, it is with the express understanding that Westinghouse makes no representation as to completeness, accuracy, or usability of information contained therein.

BETTIS ATOMIC POWER LABORATORY
WEST MIFFLIN, PENNSYLVANIA

Operated for the U. S. Department of Energy by

WESTINGHOUSE ELECTRIC CORPORATION

FOREWORD

The Shippingport Atomic Power Station located in Shippingport, Pennsylvania was the first large-scale, central-station nuclear power plant in the United States and the first plant of such size in the world operated solely to produce electric power. This project was started in 1953 to confirm the practical application of nuclear power for large-scale electric power generation. It has provided much of the technology being used for design and operation of the commercial, central-station nuclear power plants now in use.

Subsequent to development and successful operation of the Pressurized Water Reactor in the DOE-owned reactor plant at the Shippingport Atomic Power Station, the Atomic Energy Commission in 1965 undertook a research and development program to design and build a Light Water Breeder Reactor core for operation in the Shippingport Station. In 1976, with fabrication of the Light Water Breeder Reactor (LWBR) nearing completion the Energy Research and Development Administration established the Advanced Water Breeder Applications program (AWBA) to develop and disseminate technical information which would assist U.S. industry in evaluating the LWBR-concept. All three of these reactor development projects have been administered by the Division of Naval Reactors with the goal of developing practical improvements in the utilization of nuclear fuel resources for generation of electrical energy using water-cooled nuclear reactors.

The objective of the Light Water Breeder Reactor project has been to develop a technology that would significantly improve the utilization of the nation's nuclear fuel resources employing the well-established water reactor technology. To achieve this objective, work has been directed toward analysis, design, component tests, and fabrication of a water-cooled, thorium oxide fuel cycle breeder reactor to install and operate at the Shippingport Station. Operation of the LWBR core in the Shippingport Station started in the Fall of 1977 and is expected to be completed in about 3 to 4 years. Then the fissionable fuel inventory of the core will be measured. This effort, when completed in about 2 to 3 years after completion of LWBR core operation, is expected to confirm that breeding actually took place.

The Advanced Water Breeder Applications (AWBA) project was initiated to develop and disseminate technical information that will assist U.S. industry in evaluating the LWBR concept for commercial-scale applications. The project will explore some of the problems that would be faced by industry in adapting technology confirmed in the LWBR program. Information to be developed includes concepts for commercial-scale prebreeder cores which will produce uranium-233 for light water breeder cores while producing electric power, improvements for breeder cores based on the technology developed to fabricate and operate the Shippingport LWBR core, and other information and technology to aid in evaluating commercial-scale application of the LWBR concept.

Technical information developed under the Shippingport, LWBR, and AWBA projects has been and will continue to be published in technical memoranda, one of which is this present report.

TABLE OF CONTENTS

LIST OF TABLES

LIST OF ILLUSTRATIONS

LIST OF ILLUSTRATIONS (Cont)

NOMENCLATURE

Symbol	Definition
$\dot{a}$	Gas generation rate (atom fraction per second)
A	$1.19 \times 10^{-22} \exp(-100\,000/RT) cm^5/sec$ for UO_2; $1.19 \times 10^{-22} \exp(-125\,000/RT)\ cm^5/sec$ for ThO_2
$\dot{a}_b$	Rate that gas atoms go to the grain boundaries in atom fraction per second of grain boundary sites
$\dot{a}_c$	Rate at which gas atoms migrate to corner bubbles
$\dot{a}_e$	Rate at which gas arrives at the grain edge from the boundary (in atom fraction per second)
b	Tunnel radius (cm)
b'	3.86×10^{-8} cm, Burgers vector for UO_2; 3.52×10^{-8} cm for ThO_2 (See λ)
B_b	$\left(\frac{kT}{2\gamma\alpha \sin\varphi}\right)^{1/2}$
C	Gas concentration in grain interior (in atom fraction)
C'	Probability that a bubble lattice site is occupied by a bubble
$<C>$	Average gas concentration in grain interior (in atom fraction)
C_b	Grain boundary gas atom concentration (in atom fraction)
C_b'	Fraction of grain boundary bubble sites occupied by grain boundary bubbles
$<C_b>$	Average gas concentration on the boundary (in atom fraction)
C_c	Concentration of isolated gas atoms beyond which nucleation of permanent bubbles will occur (in atom fraction)
C_e	Gas concentration at grain boundary edges (in atom fraction)
C_e'	Fraction of grain boundary edge bubble sites occupied by grain boundary edge bubbles (in atom fraction)
C_I	Concentration of single gas atoms in matrix (in atom fraction)
C_{I_b}	Concentration of isolated grain boundary gas atoms (in atom fraction)
C_o	$\exp(-47\,000/RT)$, equilibrium vacancy concentration for UO_2; $\exp(-58\,750/RT)$ for ThO_2 (in atom fraction)
C_v	Vacancy concentration (in atom fraction)
D	Gas diffusion coefficient (cm^2/sec)
D_b	Bubble diffusion coefficient (cm^2/sec)

NOMENCLATURE (Cont)

Symbol	Definition
D_g	$7.6 \times 10^{-6} \exp(-71\,500/RT) + (2.5 \times 10^{-7})^2/6\tau$, gas atom diffusion coefficient for UO_2; $7.6 \times 10^{-6} \exp(-89\,375/RT) + (2.5 \times 10^{-7})^2/6\tau$ for ThO_2 (cm^2/sec)
D_{gb}	$3 \exp(-34 \times 10^3/T)$ cm^2/sec, self-diffusion coefficient along the grain boundary for UO_2; $3 \exp(-43 \times 10^3/T)$ (cm^2/sec) for ThO_2
D_i	$(10^{13})(3.86 \times 10^{-8})^2 \exp[-(0.3)(23\,050)/RT]/6$, interstitial diffusion coefficient (cm^2/sec)
D_s	$560 \times 10^4 \exp(-5.95 \times 10^4/T)$ cm^2/sec, surface self-diffusion coefficient for UO_2; $560 \times 10^4 \exp(-7.44 \times 10^4/T)$ cm^2/sec for ThO_2
D_v	$3 \times 10^{-2} \exp(-47\,000/RT)$ cm^2/sec, vacancy diffusion coefficient for UO_2; $3 \times 10^{-2} \exp(-58\,750/RT)$ cm^2/sec for ThO_2
D_{v_g}	Vacancy diffusion coefficient along the grain boundaries (cm^2/sec)
E_ℓ	$0.719\ R_g$, grain edge length (cm)
f	Total fraction of gas released
$\dot{f}$	Fission rate (in fissions/cm^3 sec)
f_b	Relative grain boundary bubble jump frequency (sec^{-1})
k	1.38×10^{-16}, Boltzmann's constant (erg deg^{-1})
m	Number of gas atoms per cm^3
$<m>$	Number of gas atoms in the matrix per cm^3
m_b	Number of gas atoms per cm^2 of boundary
m_e	Number of gas atoms on grain boundary edge per cm of edge
n	Number of gas atoms in a bubble
$\bar{n}$	Number of jumps a bubble makes before coalescence
N′	Number of matrix bubbles per cm^3
N″	Maximum number of atoms in a matrix bubble just before coalescence
$<N>$	Average number of gas atoms in a bubble
n_b	Number of atoms in a grain boundary bubble
$<n_b>$	Average number of gas atoms in a grain boundary bubble
n_b'	Number of jumps a grain boundary bubble makes
$\bar{n}_b'$	Number of jumps a grain boundary bubble makes before coalescence

NOMENCLATURE (Cont)

Symbol	Definition
N_b	Number of gas atoms in a boundary bubble at destruction
$<N_b>$	Average number of bubbles on the grain boundary per cm^2
N'_b	Number of bubbles per cm^2 of grain boundary
n_c	Number of atoms in a matrix bubble of radius 25Å
n'_c	Number of atoms in a corner bubble
N_d	Number of damage cascades per cm^3
n_e	Number of gas atoms in an edge bubble
$<n_e>$	Average number of atoms in grain edge bubble
$\underline{n}_e$	Number of gas atoms in an edge bubble at destruction by fission fragment
n'_e	Number of grain boundary edge bubble jumps
$\bar{n}'_e$	Number of grain boundary edge bubble jumps to coalescence
N_e	Number of gas bubbles per unit length of grain boundary edge (one unit length equals 1 cm)
$<N_e>$	Average number of bubbles on the grain edge per cm
n_g	Number of gas atoms in an intragranular pore
N_o	Ω^{-1} = Number of lattice sites per cm^3
N_p	Number of intragranular fabrication pores per cm^3
N'_p	Number of initial grain boundary fabrication pores per cm^3
P	External pressure (dynes/cm^2)
P_g	Fission gas pressure within the intragranular pores (dynes/cm^2)
P'_g	Gas pressure in corner pores (dynes/cm^2)
Q^*	100 000 cal/mole, heat of transport for UO_2; 125 000 cal/mole for ThO_2
r	Bubble radius (cm)
$<r>$	Average bubble radius (cm)
$\bar{R}$	Radius of grain boundary bubble curvature (cm)
R'	Half the distance between grain boundary bubbles (cm)
r_b	Grain boundary bubble radius (cm)

NOMENCLATURE (Cont)

Symbol	Definition
$\langle r_b \rangle$	Average grain boundary bubble radius (cm)
R_b	$\frac{2}{\sqrt{14}}$ R_g (cm), grain face radius
r_c	Radius of grain corner bubble (cm)
r_d	Radius of collapsed vacancy loop assumed to represent damage cascade (cm)
r_e	Radius of grain boundary edge bubble (cm)
$\langle r_e \rangle$	Average grain boundary edge bubble radius (cm)
R_g	Grain radius (cm)
r_p	Intragranular fabricated pore radius (cm)
r_p'	Corner pore radius (cm)
T	Absolute temperature (°K)
t_n	Time for a bubble containing n atoms to coalesce (sec)
V	Grain boundary bubble volume (cm^3)
α	1.587 (unitless)
β	6.97×10^{-23} cm^3, van der Waals gas constant
Γ	Bubble jump frequency (cm^{-1})
γ	626 ergs/cm^2, surface tension for UO_2; 775 ergs/cm^2 for ThO_2
γ_{Gb}	Grain boundary energy (ergs/cm^2)
δ	$\left(\frac{3\beta}{4\pi}\right)^{1/3}$
δ'	Distance from grain boundary (10Å) in which grain boundary diffusion takes place
Δt	Time step (sec)
∇T	Temperature gradient (°C/cm)
ϵ	0.05, size misfit parameter (unitless)
η	Number of vacancies knocked out of a pore per collision with fission fragment
λ	3.86×10^{-8} cm for UO_2; 3.52×10^{-8} cm for ThO_2
λ'	Viable fission fragment length for causing displacements (10^{-4} cm)

NOMENCLATURE (Cont)

Symbol	Definition
μ	7.2×10^{11} dynes/cm^2, shear modulus
ν	Poisson's constant
ξ	$\left(\frac{kT}{8\gamma\pi}\right)\left(\frac{4\pi}{3\beta}\right)^{1/3}$
ξ'	Number of vacancies escaping two damage cascades
ρ'	Dislocation density (cm^{-2})
ρ_b	Distance from center of grain face (cm)
τ	Mean stay time of a lattice atom between two fission events (sec)
φ	Angle between grain boundary and bubble surface
Ω	4.1×10^{-23} cm^3, atomic volume for UO_2; 4.38×10^{-23} (cm^3) for ThO_2

A model was developed to predict in-pile fission gas swelling, gas release, and densification in oxide fuels. This model considers fission gas behavior at the grain interior, on the grain boundaries, and at grain boundary edges under conditions of total gas bubble destruction by fission fragments and partial gas bubble destruction. When gas bubble swelling on grain edges reaches 5 percent, it is assumed that gas tunnels form along the edges. Gas release takes place by migration of the gas in the grains and on the grain boundaries to the edge tunnels. Intergranular and intragranular densifications are considered. Densification takes place by vacancy boil-off due to thermal excitation and vacancy knockout by the passage of fission fragments through the pores. The migration rates of both vacancies and interstitials to pores are also calculated. Comparisons are made between the model and experimental data for swelling, gas release, and densification and found to be in reasonable agreement in most cases.

A MODEL TO PREDICT SWELLING, GAS RELEASE, AND DENSIFICATION IN OXIDE FUELS

(AWBA Development Program)

C. C. Dollins

I. INTRODUCTION

This report describes a model for calculating swelling due to fission gas and solid fission products, gas release, and densification of fabricated porosity in oxide fuels. The model keeps track of the location of the gas in the fuel and assumes that gas migrates from the grain interior to grain boundaries, along grain boundaries to grain edges, and along grain edges to grain corners. Once the gas swelling due to bubbles on the grain edges and at the corners exceeds 5 percent, tunnels form along the grain edges and gas release occurs. There are seven regions or conditions in the fuel where gas behavior is considered:

1. Small intragranular gas bubbles (radius, r < 25Å), which can be destroyed by a single fission fragment
2. Large intragranular gas bubbles (r > 25Å), which cannot be destroyed by a single fission fragment
3. Small grain boundary gas bubbles (r_b < 25Å), which can be destroyed by a single fission fragment
4. Large grain boundary gas bubbles (r_b > 25Å), which cannot be destroyed by a single fission fragment
5. Grain boundary edge bubbles which can always be destroyed, since they never get larger than the 25Å cutoff radius
6. Corner bubbles which can never be destroyed, since any gas knocked from them immediately funnels back to the grain corners along the grain boundaries
7. Tunnels along grain edges, which result in gas escape.

II. MODEL DESCRIPTION

A. Grain Interior Gas Bubble Behavior for Bubble Radius <25Å

During fissioning of ^{235}U, gas is produced at the rate 0.3 atom per fission event, and during fissioning of ^{233}U at the rate 0.34 atom per fission event. This rate is treated as an atom fraction so that gas is produced for ^{235}U in the model at the rate

$$\dot{a} = 0.3\ \dot{f}\ \Omega \qquad (1)$$

where

$\dot{f}$ = the fission rate in fissions/cm^3 second
Ω = the atomic volume (4.1×10^{-23} cm^3).

It is assumed that the fission gas is randomly or uniformly produced and is thermodynamically insoluble in UO_2. The gas forms a stable bubble nucleus when two gas atoms meet. The bubbles increase in size by coalescing. The bubble lifetime is limited to the time between two fission events in the same region, τ, which is given in Reference 1 by

$$\tau = (1.0 \times 10^5\ \Omega\ \dot{f}\ )^{-1} \qquad (2)$$

It is then assumed that the gas bubbles are completely destroyed and the gas is driven randomly back into solution. Such a model will not be correct if the bubbles are larger than r = 25Å because a single fission event would be unable to destroy the bubbles. Consequently, the model is limited to low temperatures where bubble migration is

sufficiently slow to prevent the bubble radius from becoming larger than 25Å.

In order to calculate swelling and long-range migration, it is necessary to calculate the average bubble radius and the number of bubbles present.

It is assumed that the gas pressure within a bubble is in equilibrium with the surface tension so that van der Waals gas law can be written approximately as

$$\frac{2\gamma}{r}\left(\frac{4}{3}\pi r^3 - n\beta\right) = nkT \ , \qquad (3)$$

where

- r = bubble radius
- γ = surface tension (not temperature dependent)
- n = number of gas atoms in the bubble
- β = van der Waals constant (6.97×10^{-23} cm^3)
- k = Boltzmann's constant (1.38×10^{-16})
- T = absolute temperature.

For purposes of this report, it is necessary to solve Equation (3) for r. At low temperatures and small n (which is expected for a model with complete bubble destruction), r is given by

$$r \simeq \left(\frac{3n\beta}{4\pi}\right)^{1/3} + \frac{nkT}{8\gamma\pi}\left(\frac{4\pi}{3n\beta}\right)^{1/3}$$

or

$$\simeq \delta n^{1/3} + \xi n^{2/3} \ , \qquad (4)$$

where the second term is smaller than the first.

To calculate the number of atoms in a bubble, it will be assumed that immediately after a fission fragment passes through a region the isolated gas atoms in that region migrate until they collide with one another, forming two-atom bubbles. The two-atom bubbles migrate until they collide, forming four-atom bubbles, etc. It will be assumed that the bubbles lie on a simple cubic "bubble lattice" with a lattice spacing of 2r. The average number of jumps that a bubble makes before coalescence (Reference 2) is

$$\bar{n} = 1.52/C' \ , \qquad (5)$$

where C' is the probability that a bubble lattice site is occupied by a bubble. If N' is the number of bubbles per unit volume then $C' = N'(2r)^3$ and $\bar{n} = 1.52/N'(2r)^3$. The jump frequency of the bubbles on the "bubble lattice" is

$$\Gamma = 6D_b/(2r)^2 \ , \qquad (6)$$

where D_b is the bubble diffusion coefficient. The relative jump frequency for two bubbles is twice that given by Equation (6). From Reference 3, the time for a bubble of a given size to coalesce is given by

$$t_n = \frac{\bar{n}}{\Gamma} = \frac{1.52\,(2r)^2}{2N'\,(2r)^3\,6D_b} = \frac{0.063}{N'\,r\,D_b} \ . \qquad (7)$$

The time for a bubble containing n atoms to coalesce is then

$$t_n = 0.063\ n/mr\,D_b \ , \qquad (8)$$

where m is the number of gas atoms in a unit volume. If τ is the time between collisions with a fission fragment given by Equation (2), then τ is also the total time that the gas bubbles can migrate and

$$\tau = t_1 + t_2 + t_4 + t_8 + \ldots + t_{N''} \ , \qquad (9)$$

where N'' is the number of gas atoms in a bubble just before destruction. Equation (9) can be written

$$\tau = \sum_{j=0}^{\ln N''/\ln 2} t_{2j} \ . \qquad (10)$$

Using the gas bubble diffusion coefficient derived from Reference 4,

$$D_b = A/r^3 \ (cm^2/sec) \ , \qquad (11)$$

where $A = 1.19 \times 10^{-22} \exp(-100\,000/RT)$ cm^5/sec, Equation (8) becomes

$$t_n = 0.063\ nr^2/mA \ . \qquad (12)$$

From Equation (4),

$$r^2 \simeq \delta^2 n^{2/3} + 2\delta\xi n \ , \qquad (13)$$

so that

$$t_n = \frac{0.063}{mA}(\delta^2 n^{5/3} + 2\delta\xi n^2) \ . \qquad (14)$$

From Reference 3, Equation (10) then becomes

$$\tau = \int_0^{\ln N''/\ln 2} \frac{0.063}{mA}(\delta^2\, 2^{5/3j} + 2\delta\xi 2^{2j})dj \ , \qquad (14a)$$

or

$$\tau \simeq \frac{0.063\,\delta}{mA\ln 2}[3/5\delta\, N''^{5/3} + \xi N''^2] \ . \qquad (15)$$

Solving for N'' by Newton's approximation per Reference 3 yields

$$N'' = 5.72\left(\frac{\tau m\dot{A}}{\delta^2}\right)^{3/5} - 10.2\frac{\xi}{\delta}\left(\frac{\tau m\dot{A}}{\delta^2}\right)^{4/5} . \quad (16)$$

The average number of atoms in a bubble, for the time interval τ, is

$$<N> = \frac{1}{\tau}\int_0^{\tau} N'' \, dt .$$

Integrating this (Reference 3) gives

$$<N> = 6.34\frac{1}{\beta^{2/5}}(\tau m\dot{A})^{3/5} - 1.26\frac{kT}{\gamma\beta^{6/5}}(\tau m\dot{A})^{4/5} , \quad (17)$$

where the values of δ and ξ have been substituted into Equation (16). From Equation (4) the average bubble radius over the time step (Reference 3) is given by

$$<r> = \left(\frac{3<N>\beta}{4\pi}\right)^{1/3} + \frac{<N>kT}{8\gamma\pi}\left(\frac{4\pi}{3<N>\beta}\right)^{1/3} \quad (18)$$

and the swelling is given by

$$\left.\frac{\Delta V}{V}\right|_m = \frac{m}{<N>} 4/3\pi <r>^3 . \quad (19)$$

The first term in Equation (17) gives the number of gas atoms accumulated in a bubble if the gas is completely a van der Waals solid. The second term in Equation (17) is the deviation from solid or frozen gas due to high temperature or low pressure, P; that is, small $P = 2\gamma/r$ due to a large bubble radius. The fact that bubble growth is limited by fission events means that the second term in Equation (17) is much smaller than the first. The same holds true for Equation (18). Using Equations (17) and (18), the long-range migration of the gas from the grain interior to the grain boundaries can be calculated.

Using the low temperature, small bubble approximation, Equation (18) is

$$<r> \simeq (3<N>\beta/4\pi)^{1/3}$$

and Equation (17) becomes

$$<N> \simeq 6.34\frac{1}{\beta^{2/5}}(\tau m\dot{A})^{3/5} ,$$

so that

$$<r> \simeq 1.14\left(\frac{\beta\tau\dot{A}}{\Omega}\right)^{1/5} C^{1/5} , \quad (20)$$

where $C = m\Omega$ is the atom fraction gas concentration in the matrix. The average gas diffusion coefficient in the matrix is obtained by substituting $<r>$ from Equation (20) into Equation (11):

$$D \simeq \frac{\dot{A}^{2/5}}{1.51}\left(\frac{\Omega}{\beta\tau}\right)^{3/5}\frac{1}{C^{3/5}} . \quad (21)$$

In this work grains are treated as spheres of radius $\rho = R_g$, where ρ is the distance from the center of the grain. Gas migration to the grain boundaries is calculated by solving the transport equation in spherical coordinates:

$$\frac{\partial C}{\partial t} = \frac{1}{\rho^2}\frac{\partial}{\partial\rho}\left(\rho^2 D\frac{\partial C}{\partial\rho}\right) + \dot{a} , \quad (22)$$

where $C = m\Omega$ is the gas atom concentration in atom fraction and $\dot{a}$ is the gas atom generation rate.

It is assumed that the grain boundaries are perfect traps so that $C(\rho = R_g) = 0$. At these temperatures, the equilibrium gas concentration at the boundaries is on the order of 10^{-22} (units of atom fraction), which for purposes of this report is essentially zero. The other boundary condition for Equation (22) is that

$$\left.\frac{\partial C}{\partial\rho}\right|_{\rho=0} = 0 .$$

Initially, $C = 0$; therefore, from Equation (21), D is infinite. This is unreasonable. D cannot exceed D_g where D_g is the diffusion coefficient of an isolated gas atom (Reference 5) given by

$$D_g = 7.6 \times 10^{-6}\exp(-71\,500/RT) + \frac{(2.5 \times 10^{-7})^2}{6\tau} .$$

In the presence of a temperature gradient, D is augumented by D_{eff}. Both D_g and D_{eff} are functions of operating conditions. D_{eff} is given by

$$D_{eff} = \frac{2 \times 10^5 \dot{A}\pi\nabla T R_g}{9RT^2\Omega} ,$$

where ∇T is the temperature gradient in C°/cm.

B. Intragranular Bubble Behavior When the Bubble Radius >25Å

If the bubble radius is >25Å, then the gas bubbles are too large to be destroyed by a fission fragment and they grow. However, the fragments can still knock gas out of the bubbles and do it at the rate (Reference 6) n/τ where n is the number of gas atoms in the bubble. The gas that is knocked out can flow back to the bubbles at the rate $4\pi D_g C_I N_o B' n^{1/2}$, where D_g is the gas atom diffusion coefficient, C_I is the concentration of single gas atoms in atom fraction, N_o is the number of lattice atoms per unit volume, and B' is a constant relating the number of atoms in a bubble, n, to the bubble radius, r, such that

$$r = B' n^{1/2} \quad . \tag{23}$$

Hydrostatic stresses are not considered in Equation (23). They are factored in later. Equation (23) can be derived from the ideal gas law as follows:

$$\left(\frac{2\gamma}{r}\right)\frac{4}{3}\pi r^3 = nkT \quad , \tag{24}$$

where the first factor in parentheses is the gas pressure in the bubble, and the second factor on the left is the bubble volume. Equation (24) can be written

$$\frac{8\gamma\pi r^2}{3} = nkT \quad . \tag{25}$$

Equation (25) can be written

$$r = \left(\frac{3kT}{8\gamma\pi}\right)^{1/2} n^{1/2} \quad . \tag{26}$$

Therefore,

$$B' = \left(\frac{3kT}{8\gamma\pi}\right)^{1/2} \quad . \tag{27}$$

In deriving Equations (23) and (27), the ideal gas law for the larger bubbles was assumed in order to calculate the number of atoms in a bubble. Once that is known, van der Waals gas law is used to calculate the size of the bubble. This is an approximate way of taking into account external pressures, which are discussed later in this section.

The change in the concentration of single gas atoms is given in Reference 7 by

$$\frac{dC_I}{dt} = 0.3\ \dot{f}\ \Omega + \frac{N'n\Omega}{\tau} - 4\pi D_g C_I N' B' n^{1/2} \quad , \tag{28}$$

where N' is the number of bubbles per unit volume. Under conditions of interest, the isolated single gas atoms will be in steady state so that $dC_I/dt = 0$. Also $N'n\Omega/\tau >> 0.3\ \dot{f}\ \Omega$ or $0.34\ \dot{f}\ \Omega$ for ^{233}U so that from Reference 7, Equation (28) becomes

$$\frac{N'n\Omega}{\tau} = 4\pi D_g C_I N' B' n^{1/2} \quad . \tag{29}$$

Solving Equation (29) for C_I per Reference 7 gives

$$C_I = \frac{n^{1/2}\Omega}{\tau\, 4\pi D_g B'} \quad . \tag{30}$$

From Reference 7, the change in the number of gas atoms in a bubble with respect to time due to single gas atom behavior is given by

$$\frac{dn}{dt} = 4\pi D_g C_I B' N_o n^{1/2} - \frac{n}{\tau} \quad , \tag{31}$$

where N_o is the number of lattice sites per unit volume. Equation (31) is the change in the number of gas atoms per unit time due solely to behavior of single gas atoms. The number of gas atoms in a bubble can also increase due to coalescence of the bubbles. It was previously shown that the time for two bubbles containing n atoms to coalesce (Reference 3) is

$$t_n = \frac{0.063\, r^2}{N'A} = \frac{0.063\, B'^2\, n}{N'A} \quad ; \tag{32}$$

therefore,

$$\frac{dn}{dt} = \frac{2n - n}{t_n} = 15.87\frac{N'A}{B'^2} \tag{33}$$

is the rate of change of gas in a bubble due to coalescence. The total rate of change (Reference 7) is the sum of Equations (31) and (33),

$$\frac{dn}{dt} = 15.07\frac{N'A}{B'^2} + 4\pi D_g C_I B' N_o n^{1/2} - \frac{n}{\tau} \quad . \tag{34}$$

From conservation of gas,

$$N' = \frac{m - C_I N_o}{n} \quad . \tag{35}$$

Equations (30) and (35) allow C_I and N' to be defined, and therefore Equation (34) per Reference 7 can be written

$$\frac{dn}{dt} = \frac{15.87A}{B'^2}\left[\frac{C}{n\Omega} - \frac{1}{n^{1/2}\tau 4\pi D_g B'}\right] \quad , \tag{36}$$

Equation (36) does not allow for the nucleation of new gas bubbles. As the bubbles grow, the isolated gas atom concentration increases according to Equation (30). The isolated gas concentration cannot exceed that necessary to nucleate new permanent gas bubbles. The number of gas atoms in a bubble of the critical size (i.e., that which will just be able to withstand an encounter with a fission fragment) is given by solving van der Waals equation using as the critical radius the 25Å value from Reference 7 quoted earlier:

$$n_c = \frac{8\gamma\pi(2.5 \times 19^{-7})^2}{3\left(kT + \frac{2\gamma\beta}{2.5 \times 10^{-7}}\right)} \quad (37)$$

From Reference 7, putting n_c into Equation (17) and dropping the second term on the right-hand side of Equation (17), which is small compared to the first term, yields

$$n_c \cong \frac{6.34}{\beta^{2/5}}(\tau C_c N_o A)^{3/5} \quad , \quad (38)$$

where C_c is the critical concentration of isolated gas atoms beyond which nucleation of permanent bubbles will occur, thereby reducing the gas atom concentration back to C_c. Solving Equation (38) for C_c (Reference 7) gives

$$C_c = \frac{4.6 \times 10^{-2}}{\tau N_o A}(n_c \beta^{2/5})^{5/3} \quad (39)$$

From Reference 7, setting C_I equal to C_c and substituting into Equation (34) gives

$$\frac{dn}{dt} = \frac{15.87\, A\, N_o}{B'^2}\left(\frac{C - C_c}{n}\right) + 4\pi D_g C_c B' N_o n^{1/2} - \frac{n}{\tau} \quad (40)$$

Equation (40) is difficult to solve even by numerical methods; however, the steady-state equation obtained by setting $dn/dt = 0$ is much easier to solve. It must be shown that $dn/dt \approx 0$ is valid. If it is valid at low temperatures, then it must be valid at higher temperatures where bubble and gas diffusion are much more rapid. At 1300°C (at lower temperatures large bubbles do not form) and for a fission rate of 10^{13} fissions/cm^3 second and using the values of the parameters given in the Nomenclature, C_c is 3.89×10^{-3} and n_c is 579. At a depletion of 4×10^{20}, C is equal to 5.59×10^{-3} for $\dot{f} = 10^{13}$ fissions/cm^3 second. Using n equal to n_c the first term on the right-hand side of Equation (40) is equal to 0.0373 and the second term is 0.150. At equilibrium when $dn/dt = 0$, the first term on the right-hand side is equal to 0.00093 and the second term is equal to 0.951. Consequently, under these conditions the first term on the right-hand side can be ignored. From Reference 7 the solution of the remaining equation,

$$\frac{dn}{dt} = 4\pi D_g C_c B' N_o n^{1/2} - \frac{n}{\tau} \quad , \quad (41)$$

is

$$n_2 = [4\pi D_g C_c B' N_o \tau - (4\pi D_g C_c B' N_o \tau - n_1^{1/2}) \exp(-\Delta t/2\tau)]^2 \quad , \quad (42)$$

where n_1 is the initial number of gas atoms in the bubble and n_2 is the number of gas atoms in the bubble Δt later. The value n_2 is reached on the order of 2τ, which for a fission rate of 10^{13} fissions/cm^3 second is about seven hours. In seven hours the depletion is going to change very little and hence C is going to change very little; thus, setting dn/dt equal to zero is a good approximation. In the initial stages n is very small, making the first term on the right-hand side of Equation (40) large. This produces an even more rapid advance to steady state. From Reference 7, Equation (40) now becomes

$$\frac{15.87\, A\, N_o}{B'^2}\left(\frac{C - C_c}{n}\right) + 4\pi D_g C_c B' n^{1/2} N_o - \frac{n}{t} = 0 \quad . \quad (43)$$

The roots of Equation (43) can be found analytically but with difficulty. The roots can be found easily on a computer using the Newton-Raphson method. Setting the left-hand side of Equation (43) equal to F(n), an iteration scheme can be written

$$n_1 = n_o - \frac{F(n_o)}{F'(n_o)} \quad , \quad (44)$$

where $F'(n_o)$ is the first derivative of F with respect to n evaluated at n_o. The initial value of n_o comes from the previous time step. Once n, the number of gas atoms in a bubble is known, the bubble radius is calculated from van der Waals gas law. The number of bubbles per unit volume is given by

$$N' = \frac{N_o(C - C_c)}{n} \quad . \quad (45)$$

The swelling is given by

$$\left.\frac{\Delta V}{V}\right|_m = \frac{4}{3}\pi r^3 N' + \beta C_c N_o \quad . \quad (46)$$

The average gas diffusion coefficient is given by

$$D = \frac{\frac{A}{r^3}N'n + C_c N_o D_g}{N_o C} + D_{eff} \quad . \qquad (47)$$

The diffusion coefficient given by Equation (47) is that used in Equation (22) to calculate the amount of gas that migrates to the grain boundaries and the amount remaining in the interior of the grains. As before, D is not allowed to exceed D_g.

In the computer program, the small matrix gas bubble and large matrix gas bubble calculations are combined.

For the large bubbles ($r > 25$Å), the number of atoms in the bubbles is first calculated and then their radii using van der Waals gas law:

$$\frac{4}{3}\pi \rho r^4 + 8\frac{\gamma}{3}\pi r^3 - r(Pn\beta + nkT) - 2\gamma n\beta = 0 \quad (47a)$$

where P is the external pressure (dynes/cm^2).

The rate that gas leaves the matrix and migrates to the grain boundary, $\dot{a}_b$, is given by

$$\dot{a}_b = \left(\dot{a} - \frac{\Delta C}{\Delta t}\right)\frac{2R_g}{3\gamma} \quad ,$$

where

γ = atomic jump distance
ΔC = change in the average gas concentration in the grain interior, in units of atom fraction
Δt = time step over which ΔC is measured.

The average gas concentration in the grain interior is given by

$$\langle C \rangle = \frac{1}{\frac{4}{3}\pi R_g^3}\int_0^{R_g} C(\rho) 4\pi \rho^2 \, d\rho \quad .$$

Grain boundary swelling and gas migration can now be calculated.

C. Grain Boundary Gas Bubble Swelling and Gas Migration for Bubble Radius <25Å

A gas bubble on a grain boundary will be lens shaped due to the grain boundary energy, assuming it approximates an equilibrium shape. The angle the bubble makes at the grain boundary, φ, is related to the grain boundary energy by the equation

$$\cos\varphi = \frac{\gamma_{Gb}}{2\gamma} \quad . \qquad (48)$$

If r_b is the radius of the bubble on the grain boundary and $\bar{R}$ is the actual radius of curvature of the bubble, then

$$r_b = \bar{R}\sin\varphi \quad . \qquad (49)$$

Assuming that the gas pressure within the bubble equilibrates with the surface tension, then $P = 2\gamma/R$, so that

$$P = \frac{2\gamma \sin\varphi}{r_b} \quad . \qquad (50)$$

The volume of the bubble is given by

$$V = \frac{2}{3}\pi r_b^3 \frac{(1 - \cos\varphi)(2 + \cos\varphi)}{\sin\varphi(1 + \cos\varphi)} \quad ,$$

or

$$V = \alpha r_b^3 \quad . \qquad (51)$$

van der Waals gas law is given by

$$P(V - n_b\beta) = n_b kT \quad , \qquad (52)$$

where n_b is the number of gas atoms in the bubble. Substituting Equations (50) and (51) into (52) gives

$$\frac{2\gamma \sin\varphi}{r_b}(\alpha r_b^3 - n_b\beta) = n_b kT \quad . \qquad (53)$$

From Reference 7, solving Equation (53) for r_b in the case of small bubbles gives

$$r_b \cong \left(\frac{\beta}{\alpha}\right)^{1/3} n_b^{1/3} + \frac{n_b kT}{6\gamma \sin\varphi\alpha}\left(\frac{\alpha}{n_b\beta}\right)^{1/3} \quad , \qquad (54)$$

which can be written

$$r_b \cong \delta_b n_b^{1/3} + \xi_b n_b^{2/3} \quad . \qquad (55)$$

Fission fragments are able to knock gas atoms from the grain boundaries but only for distances of approximately 15Å; because of the extensive nature of the grain boundary it is expected that the gas atoms will return to the boundary and not be able to escape. Consequently, gas buildup on the boundary becomes quite large. As in the case of the grain interior, it is assumed that grain boundary bubbles obey van der Waals gas law and that they can be completely destroyed by a single fission fragment.

In order to calculate bubble growth on the boundary, it is necessary to develop a technique similar to that used for grain interior.

As before, assume a square "bubble lattice" on the grain boundary with lattice parameter $2r_b$,

where r_b is the grain boundary bubble radius. The concentration, C'_b, of gas bubbles is the fraction of sites occupied by bubbles. If S_n is the number of new sites visited after n'_b jumps, then the number of jumps to coalescence, $\bar{n}'_b$, is calculated by solving the equation

$$1 = \int_0^{\bar{n}'_b} b \frac{\partial S_n}{\partial n'_b} C'_b dn'_b \quad . \tag{56}$$

For random walk confined to a plane, Dvoretzky and Erdos (Reference 8) found

$$S_n = \pi n'_b / \ln n'_b \quad , \tag{57}$$

where n'_b is a very large number. For n'_b less than about 23, Equation (57) indicates that the number of new sites visited is greater than the number of jumps and so Equation (57) is not adequate for the case herein, where a small number of jumps is expected. For use in this report, Equation (57) is approximated by

$$S_n = n_b^{0.89} \quad , \tag{58}$$

which agrees with Equation (57), within 5 percent over nearly four orders of magnitude up to $n'_b = 10^6$. Equation (58) also has the benign result of giving one new site visited by the first jump, unlike Equation (57). Substituting S_n from Equation (58) into Equation (56) and solving yields

$$n'_b = C'^{-1.12}_b \tag{59}$$

as the number of jumps a gas bubble must make to coalesce with another gas bubble of the same size. Since

$$C'_b = N'_b (2r_b)^2 \quad ,$$

where N'_b is the number of bubbles per unit area of grain boundary,

$$n'_b = [N'_b (2r_b)^2]^{-1.12} \quad .$$

The relative jump frequency between two bubbles confined to motion in a plane is

$$f_b = 8D_b/(2r_b)^2 \quad .$$

As before, it can be shown from Reference 3 that the lifetime of a bubble containing n_b atoms is

$$t_n = \frac{\bar{n}'_b}{f_b} = \frac{n_b^{1.12} r_b^{2.76}}{9.45\, Am_b^{1.12}} \quad , \tag{60}$$

where Equation (11) is assumed, and m_b is the number of gas atoms per unit area of boundary. The bubble radius, r_b, is given by Equation (55) and $r_b^{2.76}$ is given by

$$r_b^{2.76} = \delta_b^{2.76} n_b^{0.92} + 2.76\, \delta_b^{1.76} \xi_b n_b^{1.25} \tag{61}$$

From Reference 3, Equation (60) then becomes

$$t_n = \frac{\delta_b^{1.76}}{9.45\, Am_b^{1.12}} (\delta_b n_b^{2.04} + 2.76\, \xi_b n_b^{2.37}) \quad .$$

After integrating as in Equation (14a), it is found that the time interval, τ, for grain boundary bubbles to grow until they contain N_b atoms (Reference 3) is

$$\tau \simeq \frac{\delta_b^{1.76}}{9.45\, Am_b^{1.12}} \left[\frac{\delta_b}{2.04} \frac{N_b^{2.04}}{\ln 2} + \frac{1.165}{\ln 2} \xi_b N_b^{2.37} \right] \quad .$$

From Reference 3, solving for N_b by Newton's approximation yields

$$N_b = \left(\frac{13.36\, Am_b^{1.12}\, \tau}{\delta_b^{2.76}} \right)^{0.49} - 1.164 \frac{\xi_b}{\delta_b} \left(\frac{13.36\, Am_b^{1.12}\, \tau}{\delta_b^{2.76}} \right)^{0.65} \quad .$$

From Reference 3, averaging over a time interval, τ, yields

$$\langle n_b \rangle = 2.39 \left(\frac{Am_b^{1.12} \tau}{\delta_b^{2.76}} \right)^{0.49} - 3.8 \frac{\xi_b}{\delta_b} \left(\frac{Am_b^{1.12} \tau}{\delta_b^{2.76}} \right)^{0.65} \quad , \tag{62}$$

as the average number of atoms in a grain boundary bubble where m_b is the number of gas atoms on the grain boundary per unit area. The second term on the right-hand side of Equation (62) is much smaller than the first. The average grain boundary bubble radius, $\langle r_b \rangle$, is given by substituting $\langle n_b \rangle$ into Equation (5), and the average grain boundary gas diffusion coefficient, D_b, is given by substituting $\langle r_b \rangle$ into Equation (11):

$$D_b = \frac{A}{\langle r_b \rangle^3} \quad . \tag{63}$$

With knowledge of the long-range grain boundary gas diffusion coefficient, migration of the gas in the grain boundaries to grain boundary edges can be calculated. If it is assumed that the grains are tetrakaidecahedrons and, if it is further assumed that each of the fourteen faces has equal area, then the area of one grain face is equal to $4\pi R_g^2/14$. The radius of the face is given by

$$R_b = \frac{2}{\sqrt{14}} R_g \quad , \tag{64}$$

where R_g is the grain radius.

It is assumed that the grain edges are perfect traps for the grain faces so that the concentration at the grain edges is equal to zero. Gas motion on the grain faces can be determined by solving the transport equation using polar coordinates:

$$\frac{\partial C_b}{\partial t} = \frac{1}{\rho_b} \frac{\partial}{\partial \rho_b} \left(\rho_b D_b \frac{\partial C_b}{\partial \rho_b} \right) + \dot{a}_b \quad , \tag{65}$$

where ρ_b is the distance from the center of the grain face. The boundary conditions for Equation (65) are $C_b(\rho_b = R_b) = 0$ and

$$\left. \frac{\partial C_b}{\partial \rho_b} \right|_{\rho b = 0} = 0 \quad .$$

As before, D_b should not exceed D_g.

Under certain conditions the gas concentration on the boundaries can build up to the point where the bubbles can form a connected path to the grain edge. It is assumed that when this occurs gas is drained completely out of the grain boundary to the edge and the boundary heals. Gas can then build up again in the boundary and when interconnectivity recurs, the gas is again transferred to the edge, etc. Once $\dot{a}_b$ becomes large enough that interconnection becomes frequent, then it is desirable to obtain the average swelling under those conditions.

The fraction of the grain boundary covered by bubbles is given by $\pi r_b^2 N_b'$. Transfer to the grain edge is assumed to occur when this fraction is equal to approximately 0.78 (Reference 3). For simplicity, it is assumed that transfer to the boundary edge through grain boundary gas bubble interconnectivity results in complete depletion of gas at the boundary. Define t_r as the time necessary to build the gas concentration from zero back up to a concentration necessary for interconnect transfer to the edge and t is the time in this interval since the last complete transfer to the edge. The number of gas atoms per unit area on the boundary will be given by

$$m_b = \dot{a}_b \, t \, \lambda / \Omega \quad . \tag{66}$$

From Reference 7, the number of gas atoms in the average grain boundary bubble as a function of time since the last transfer to the edge is given by substituting Equation (66) into Equation (62):

$$n_b = 2.39 \left[A \left(\frac{\dot{a}_b \, t \, \lambda}{\Omega} \right)^{1.12} \frac{\tau}{\delta_b^{2.76}} \right]^{0.49} \quad . \tag{67}$$

In Equation (67) the smaller second term of Equation (62) has been dropped. Under conditions where small grain boundary bubble interconnectivity is expected, the second term is much smaller than the first. For example, at 1000°C and at a fission rate of 10^{13} fissions/cm^3 second, and for a grain radius of 1μ, the first term of Equation (62) has a value of 25 and the second has a value of 2.6; so dropping the second term is reasonable. The number of grain boundary gas bubbles per unit area of boundary as a function of time is given in Reference 7 by

$$N_b' = \frac{\dot{a}_b \, t \, \lambda}{\Omega n_b} \quad . \tag{68}$$

From Reference 7, transfer to the edges will occur when

$$\pi r_b^2 N_b' = 0.78 \quad . \tag{69}$$

Substituting Equations (55) and (68) into Equation (69) gives (Reference 7)

$$\frac{\dot{a}_b \, t \, \lambda \, \pi \, \delta_b^2}{\Omega n_b^{1/3}} = 0.78 \quad . \tag{70}$$

Per Reference 7, substituting Equation (67) into Equation (70) and solving for t gives the time between interconnection and transfer to the grain edges, t_r, as

$$t_r = \frac{0.261 \Omega}{\dot{a}_b \, \lambda} \frac{(A\tau)^{0.2}}{\delta_b^3} \quad . \tag{71}$$

From Reference 7, the average number of gas atoms in a grain boundary bubble is given by solving

$$\langle n_b \rangle = \frac{1}{t_r} \int_0^{t_r} n_b \, dt \quad , \tag{72}$$

where n_b is given by Equation (67). From Reference 7, the integral in Equation (72) reduces to

$$\langle n_b \rangle = 1.54 \left[\frac{A\tau}{\delta_b^{2.76}} \right]^{0.49} \left(\frac{\dot{a}_b \, \lambda}{\Omega} \right)^{0.5488} t_r^{0.5488} \quad . \tag{73}$$

The average number of bubbles on the grain boundary per unit area (Reference 7) is

$$\langle N_b \rangle = \frac{\dot{a}_b\, t_r\, \lambda}{2\Omega \langle n_b \rangle} \quad (74)$$

The total grain boundary swelling per unit volume is given by multiplying the grain boundary area per unit volume by the swelling per unit area. The grain boundary area per unit volume is equal to $3/(2R_g)$, where R_g is the grain radius. The swelling per unit volume due to the grain boundary bubbles is given by

$$\left.\frac{\Delta V}{V}\right|_b = \frac{3}{2R_g}\,\alpha\, r_b^3 \langle N_b \rangle \quad (75)$$

The average gas concentration on the grain boundary is given by

$$\langle C_b \rangle = \langle n_b \rangle \langle N_b \rangle \frac{\Omega}{\lambda} \quad (76)$$

D. Grain Boundary Gas Bubble Swelling and Gas Migration for Bubble Radius >25Å

The previous section assumes complete grain boundary bubble destruction; however, quite early, even at relatively low temperatures, grain boundary bubbles become too large to be destroyed by a single encounter with a fission fragment.

As in the case of the large intragranular bubbles, the ideal gas law is assumed to hold for the large grain boundary bubbles when the number of atoms in a bubble is calculated. As before, gas is knocked out of the grain boundary bubbles at the rate

$$\frac{n_b}{\tau} \quad (77)$$

As stated in Reference 7, isolated grain boundary gas atoms migrate to the grain boundary bubbles at the rate

$$\frac{2\pi D_g C_{Ib} \lambda}{\ln(R'/r_b)\,\Omega}, \quad (78)$$

where C_{Ib} is the concentration of isolated grain boundary gas atoms and R' is half the distance between grain boundary bubbles. In steady state the rates given by Equations (77) and (78) are equal, and therefore, from Reference 7,

$$C_{Ib} = \frac{n_b\,\Omega}{2\pi\,\tau\, D_g\,\lambda} \ln\left(\frac{R'}{r_b}\right). \quad (79)$$

The large gas bubbles obey the ideal gas law to close approximation; therefore, the bubble radius is given by

$$r_b = \left(\frac{kT\, n_b}{2\gamma\alpha \sin\varphi}\right)^{1/2} = B_b\, n_b^{1/2} \quad (80)$$

The grain boundary bubbles can also grow by coalescence. As stated in Reference 3, the lifetime of a bubble containing n_b atoms is

$$t_{n_b} = \frac{n_b^{1.12}\, r_b^{2.76}}{9.45\, A (N_b'\, n_b)^{1.12}}, \quad (81)$$

where N_b' is the number of gas bubbles per unit area. From Reference 7, substituting Equation (80) into (81) gives

$$t_{n_b} = \frac{B_b^{2.76}\, n_b^{1.38}}{9.45\, A\, N_b'^{1.12}}. \quad (82)$$

Since

$$\frac{dn_b}{dt} = \frac{2n_b - n_b}{t_{n_b}}, \quad (83)$$

then due to coalescence (Reference 7),

$$\frac{dn_b}{dt} = \frac{9.45\, A\, N_b'^{1.12}}{B_b^{2.76}\, n_b^{0.38}}. \quad (84)$$

According to Reference 7, the total rate of change of the gas in a bubble can be written

$$\frac{dn_b}{dt} = \frac{9.45\, A\, N_b'^{1.12}}{B_b^{2.76}\, n_b^{0.38}} + \frac{2\pi D_g C_{Ib} \lambda}{\ln(R'/r_b)\,\Omega} - \frac{n_b}{\tau}. \quad (85)$$

From the steady-state conditions of Equation (79), the last two terms of Equation (85) cancel and from conservation of matter

$$N_b' = \frac{\lambda}{\Omega\, n_b}(C_b - C_{Ib}). \quad (86)$$

For small bubbles $C_b >> C_{Ib}$, so the C_{Ib} term of Equation (86) will be dropped. For UO_2 fissioning at 10^{13} fissions/cm^3 second at 1000°C and for a grain radius of 1μ, we have $C_b = 0.35$ and $C_{Ib} = 0.01$; therefore, the approximation is reasonable. Equation (85) now, per Reference 7, becomes

$$\frac{dn_b}{dt} = \frac{9.45\, A}{B_b^{2.76}\, n_b^{3/2}} \left(\frac{\lambda\, C_b}{\Omega}\right)^{1.12}. \quad (87)$$

Equation (87) can be integrated (Reference 7) to give

$$n_{b_2} = \left[\frac{23.6\,A}{B_b^{2.76}}\left(\frac{\lambda}{\Omega}\right)^{1.12} C_b^{1.12}\,\Delta t + n_{b_1}^{5/2}\right]^{2/5} \quad (88)$$

where n_{b_2} is the number of atoms in a bubble, initially containing n_{b_1} atoms, after a time Δt. Using r_b calculated from Equation (88), the bubble radius can be obtained, and hence the bubble diffusion coefficient. Knowing the bubble diffusion coefficient, Equation (65) can be solved and gas migration to the grain edges can be predicted. The grain boundary bubble radius is

$$P\alpha r^4 + 2\gamma\alpha r^3 - (Pn\beta - nkT)r - 2\gamma n\beta = 0 \quad (89)$$

Equation (89) is then solved in exactly the same fashion as Equation (47a).

Equation (88) is valid only as long as the gas bubbles on the boundary cannot form an interconnected path to the grain edge; in the low temperature case that may happen very soon. Once $\dot{a}_b$ becomes large enough that interconnection becomes frequent, it is then desirable to obtain the average swelling under those conditions as before.

As reported in Reference 3, the gas on the boundaries is transferred to the grain edges when $\pi B_b^2 \lambda C_b/\Omega \simeq 0.78$. From Reference 7, this gives C_b upon transfer as

$$C_b = \frac{0.78\Omega}{\pi B_b^2 \lambda} \quad (90)$$

Gas arrives at the boundary at the rate $\dot{a}_b$ so that the time it takes to transfer the gas from boundary to edge (Reference 7) is

$$t_r = \frac{0.78\Omega}{\pi B_b^2 \lambda \dot{a}_b} \quad (91)$$

The average number of gas atoms in a grain boundary bubble is given by solving Equation (72), where n_b is given by solving a modified Equation (87) (Reference 7):

$$\frac{dn_b}{dt} = \frac{9.45\,A}{B_b^{2.76}\,n_b^{3/2}}\left(\frac{\lambda\,\dot{a}_b}{\Omega}\right)^{1.12} t^{1.12} \quad (92)$$

To obtain $n_b(t)$, Equation (92) is integrated (Reference 7):

$$\int_0^{n_b} n_b^{3/2}\,dn_b = \int_0^t \frac{9.45\,A}{B_b^{2.76}}\left(\frac{\lambda\,\dot{a}_b}{\Omega}\right)^{1.12} t^{1.12}\,dt \quad (93)$$

From Reference 7, upon solution,

$$n_b = \left[11.1\,\frac{A}{B_b^{2.76}}\left(\frac{\lambda\,\dot{a}_b}{\Omega}\right)^{1.12} t^{2.12}\right]^{2/5} \quad (94)$$

Substituting Equation (94) into Equation (72), $\langle n_b \rangle$ is obtained (Reference 7):

$$\langle n_b \rangle = \left[\frac{2.39\,A}{B_b^{2.76}}\left(\frac{\lambda\,\dot{a}_b}{\Omega}\right)^{1.12} t_r^{2.12}\right]^{2/5} \quad (95)$$

From Reference 7, substituting Equation (91) into Equation (95) gives

$$\langle n_b \rangle = \left[\frac{1.41\,A\,\Omega}{\dot{a}_b\,\pi^{2.12}\,B_b^7\,\lambda}\right]^{2/5} \quad (96)$$

The average number of bubbles per unit area of boundary is given by Equation (74), which is equal to (Reference 7)

$$\langle N_b \rangle = \frac{0.78}{2\pi B_b^2 \langle n_b \rangle} \quad (97)$$

Knowing the bubble radius and the number of bubbles per unit area of boundary given by Equation (97), the swelling due to grain boundary bubbles can be calculated.

The average gas concentration on the grain boundary is given by

$$\langle C_b \rangle = \langle n_b \rangle \langle N_b \rangle \frac{\Omega}{\lambda} \quad (98)$$

$$= \frac{0.78\Omega}{2_0 B_b^2 \lambda} \quad (99)$$

The discussion of grain boundary gas atom behavior is complete. A discussion of grain boundary edge behavior follows.

E. Grain Edge Gas Bubble Swelling and Gas Migration

As in the case of intragranular bubbles and grain boundary bubbles, the gas bubbles on the grain edges can be destroyed by fission fragments if they are smaller than approximately 25Å radius. The dispersed gas atoms are knocked on the average about 15Å from the grain boundary and can, therefore, easily migrate back to the boundary before being trapped by other sinks. The fact that the gas bubble was originally at a boundary edge

means that when the gas atoms migrate back to the boundary they will be very close to the edge (approximately 15Å) and hence will migrate in the boundary to the edge before being captured at other traps in the boundary. Therefore, the grain edge can be treated as a perfect trap. Once back on the edge, the gas migrates nucleating new gas bubbles which in turn migrate and coalesce with one another. The gas bubbles continue to grow by coalescence until destroyed by another fission fragment.

In order to calculate grain edge bubble growth, it is necessary to develop a technique similar to that used for the intragranular bubbles and the grain boundary bubbles. The isolated gas atoms formed by the destruction of a gas bubble migrate until they collide with one another forming two-atom bubbles. The two-atom bubbles migrate until they collide, forming four-atom bubbles, etc. As in the two- and three-dimensional cases, assume a "bubble lattice" on the grain edge with lattice parameter $2r_e$ where r_e is the radius of a grain boundary edge bubble. The concentration, C'_e, of gas bubbles is the fraction of sites occupied by bubbles. If S_n is the number of new sites visited by a bubble after n'_e jumps, then the number of jumps to coalescence, $\bar{n}'_e$, is calculated by solving

$$1 = \int_0^{\bar{n}'_e} \frac{\partial S_n}{\partial n'_e} C'_e \, dn'_e \quad . \tag{100}$$

For random walk confined to a line, Vineyard (Reference 9) found

$$S_n = \left(\frac{8n'_e}{\pi}\right)^{1/2} \quad . \tag{101}$$

Substituting Equation (101) into Equation (100) and solving for $\bar{n}'_e$ yields

$$\bar{n}'_e = \frac{\pi}{8C'_e} \tag{102}$$

as the number of jumps a grain edge bubble must make to coalesce with another gas bubble of the same size. Defining N_e as the number of gas bubbles per unit length, $\bar{n}'_e$, is given by

$$\bar{n}'_e = \frac{\pi}{8N_e^2 \, 4r_e^2} \quad . \tag{103}$$

The relative jump frequency between two bubbles confined to motion on a line is

$$\Gamma = \frac{D_b}{r_e^2} \quad , \tag{104}$$

where D_b is the bubble diffusion coefficient. From Reference 7, the time for a bubble containing n_e atoms to coalesce is

$$t_{n_e} = \frac{\bar{n}'_e}{\Gamma} = \frac{\pi}{32N_e^2 D_b} \quad . \tag{105}$$

The number of gas atoms on the grain edge per unit length, m_e, is given by

$$m_e = N_e \, n_e \quad . \tag{106}$$

Using this and Equation (11), Equation (105) can be written as

$$t_{n_e} = \frac{\pi \, n_e^2 \, r_e^3}{32 m_e^2 \, A} \quad . \tag{107}$$

For small bubbles the gas obeys van der Waals gas law and the bubble radius is given by Equation (4), which can be written

$$r_e = \delta n_e^{1/3} + \xi n_e^{2/3} \quad . \tag{108}$$

For bubbles smaller than approximately 25Å, the second term on the right-hand side of Equation (108) is much smaller than the first; therefore, r_e^3 can be written

$$r_e^3 = \delta^3 \, n_e + 3\delta^2 \, \xi n_e^{4/3} \quad . \tag{109}$$

Substituting Equation (109) into Equation (107) yields

$$t_{n_e} = \frac{\pi \, \delta^2}{32 m_e^2 \, A} \left(\delta n_e^3 + 3 \, \xi n_e^{10/3}\right) \quad . \tag{110}$$

The time between fission fragment damage events, τ, is given by

$$\tau = t_1 + t_2 + t_4 + t_8 + \ldots t_{n_e} \quad , \tag{111}$$

where n_e is the number of atoms in a bubble at destruction. Equation (111) can be written as

$$\tau = \sum_{j=0}^{\frac{\ln n_e}{\ln 2}} t_{2j} \quad . \tag{112}$$

The summation given by Equation (112) can be written as an integral if j is large. Substituting Equation (110) into the integral form yields

$$\tau = \frac{\pi \, \delta^2}{32 m_e^2 \, A} \int_0^{\frac{\ln n_e}{\ln 2}} \left(\delta \, 2^{3j} + 3 \, \xi \, 2^{(10/3)j}\right) dj \quad . \tag{113}$$

Equation (113) yields

$$\tau = \frac{\pi \delta^2}{32 m_e^2 A}\left[\frac{\delta \underline{n}_e^3}{3 \ln 2} + \frac{9}{10}\frac{\xi}{\ln 2}\underline{n}_e^{10/3}\right] \quad (114)$$

From Reference 7, solving Equation (114) for $\underline{n}_e$ yields

$$\underline{n}_e \cong \left(\frac{21.2 m_e^2 A \tau}{\delta^3}\right)^{3/9} - 0.899\frac{\xi}{\delta}\left(\frac{21.2 m_e^2 \tau A}{\delta^3}\right)^{4/9} \quad (115)$$

The average value of n_e, the average number of atoms in a bubble during the time interval τ, is

$$\langle n_e \rangle = \frac{1}{\tau}\int_0^{\tau} \underline{n}_e(t)dt \quad (116)$$

$\underline{n}_e(t)$ is given by substituting t for τ in Equation (116). From Reference 7, the solution of Equation (116) is

$$\langle n_e \rangle = 2.08\left(\frac{m_e^2 A \tau}{\delta^3}\right)^{3/9} - 2.42\frac{\xi}{\delta}\left(\frac{m_e^2 \tau A}{\delta^3}\right)^{4/9} \quad (117)$$

The average bubble radius, $\langle r_e \rangle$, is given by substituting $\langle n_e \rangle$ into Equation (4). The long-range diffusion coefficient of the gas is given by substituting $\langle r_e \rangle$ into Equation (11).

The gas can migrate along the grain edges to the grain corners where it is trapped. The gas migration is described by the transport equation in one dimension given by

$$\frac{\partial C_e}{\partial t} = \frac{\partial}{\partial X} D \frac{\partial C_e}{\partial X} + \dot{a}_e , \quad (118)$$

where $\dot{a}_e$ is the rate that gas arrives at the grain edge from the boundary and is given by

$$\dot{a}_e = \left(\dot{a} N_o \Delta t - \Delta C N_o - \frac{3\Delta C_b}{2R_g}\right)\frac{\Omega_g \Omega_b \lambda}{\Delta t} \quad (119)$$

where ΔC is the change in the average gas concentration in the grain interior in units of atom fraction in time Δt, and ΔC_b is the change in the gas concentration on the grain boundary in units of the fraction of boundary site occupied in time Δt. The average gas concentration on the grain boundaries is given by

$$\langle C_b \rangle = \frac{1}{\pi R_b^2}\int_0^{R_b} C_b(\rho_b)\, 2\pi \rho_b \, d\rho_b$$

where $C(\rho_b)$ is calculated from Equation (65). $\langle C_b \rangle$ may also be obtained from Equation (76) or from Equation (98), whichever is applicable.

Equation (118) is solved by a finite difference scheme similar to that for the grain interior and grain boundary cases. The edge length, $E_\ell (= 0.719 R_g)$, is the distance along the edge between grain corners. The boundary conditions for Equation (118) are $\partial C_e / \partial X = 0$ at $X = 0$, and $C_e = 0$ at $X = \pm E_\ell/2$. The grain edge swelling is given by

$$\left.\frac{\Delta V}{V}\right|_e = \frac{4\pi \langle r_e \rangle^2 \langle C_e \rangle}{3 \langle n_e \rangle R_g R_b \lambda}$$

where $\langle C_e \rangle$ is the average concentration on the edge.

Before the edge bubbles become very large, interconnection of the bubbles takes place and the gas is transported to the grain corners. This happens when C_e is approximately equal to one. The edge gas concentration then goes to zero. Gas, then, begins to accumulate again at the grain edges as before. Defining t as the time since the last interconnection event and t_r as the time between interconnection events, the edge gas concentration is given by

$$C_e = \dot{a}_e t \quad (120)$$

or, in terms of the number of gas atoms per unit length, m_e, as

$$m_e = \frac{\dot{a}_e t}{\lambda} . \quad (121)$$

Also,

$$t_r = \frac{1}{\dot{a}_e} . \quad (133)$$

Substituting m_e from Equation (121) into Equation (117) for $\langle n_e \rangle$ and dropping the smaller second term of Equation (117) yields

$$n_e = 2.08\left(\frac{\dot{a}_e^2 t^2 A \tau}{\lambda^2 \delta^3}\right)^{1/3} . \quad (123)$$

The average number of atoms in a grain edge bubble is given by

$$\langle n_e \rangle = \frac{1}{t_r} \int_0^{t_r} n_e \, dt \quad . \tag{124}$$

Substituting Equation (123) into Equation (124) and integrating (Reference 7) yields

$$\langle n_e \rangle = 1.25 \frac{(A\tau)^{1/3}}{\lambda^{2/3} \delta} \tag{125}$$

as the average number of gas atoms in a grain edge bubble once interconnectivity of edge bubbles takes place. From Reference 7, the average number of bubbles on the grain edge per unit length, $\langle N_e \rangle$, is given by

$$\langle N_e \rangle = \frac{\dot{a}_e t_r}{2\lambda \langle n_e \rangle} = \frac{\delta}{2.5 \, \lambda^{1/3} (A\tau)^{1/3}} \quad . \tag{126}$$

From Equations (125) and (126), the grain edge swelling and gas concentrations can be calculated. The average gas concentration on the edge is given by

$$\langle C_e \rangle = \frac{2}{E_\ell} \int_0^{E_\ell/2} C_e(x) dx \quad , \tag{127}$$

where $C_e(x)$ is obtained from Equation (118) or if interconnection is taking place, then $\langle C_e \rangle = 0.5$.

The average bubble radius is given by substituting $\langle n_e \rangle$ from Equation (125) into Equation (47a) and solving Equation (47a) for r.

The number of gas atoms per cm^3 in the matrix is given by

$$\langle m \rangle = \langle C \rangle N_o \quad . \tag{128}$$

The number of gas atoms per cm^3 on the grain boundaries is given by

$$\langle m_b \rangle = \langle C_b \rangle \frac{3}{2R_g \lambda^2} \quad . \tag{129}$$

The number of gas atoms per cm^3 on grain boundary edges is given by

$$\langle m_e \rangle = \frac{\langle C_e \rangle}{R_g R_b \lambda} \quad . \tag{130}$$

The total number of gas atoms in the grain corners per cm^3 is given by

$$\langle m_c \rangle = \int_0^t (0.3 \text{ or } 0.34) \, \dot{f} \, (t') dt' - \langle m \rangle - \langle m_b \rangle - \langle m_e \rangle \quad , \tag{131}$$

where the integral is the total number of gas atoms generated either from ^{235}U or ^{233}U. The number of corners per unit volume is equal to $0.695/(R_g^2 R_b)$; therefore, the number of gas atoms in a corner bubble, n_c', is given by

$$n_c' = \langle m_c \rangle R_g^2 R_b / 0.695 \quad . \tag{132}$$

The n_c' from Equation (132) can be substituted into Equation (47a) to calculate the corner bubble radius, r_c. The swelling due to the corner bubbles is given by

$$\left. \frac{\Delta V}{V} \right|_c = \frac{4}{3} \pi r_c^3 \frac{0.695}{R_g^2 R_b} \tag{133}$$

if there is no grain boundary porosity.

The total swelling is given by

$$\frac{\Delta V}{V} = \left. \frac{\Delta V}{V} \right|_m + \left. \frac{\Delta V}{V} \right|_b + \left. \frac{\Delta V}{V} \right|_e + \left. \frac{\Delta V}{V} \right|_c \quad . \tag{134}$$

F. Tunnel Formation

At low temperatures the gas is confined primarily to the grain interiors. At higher temperatures the gas migrates to the boundaries, edges, and corners where the bubbles can become very large. It has been observed that tunnels form along the grain boundary edges when the swelling of corner and edge bubbles exceeds 5 percent. It is further assumed that gas that migrates to the tunnels escapes from the fuel and is released.

The tunnels once formed have a tendency to heal by sintering. The tunnels can grow if the number of vacancies brought to them by the gas bubbles from the grain boundaries exceeds the vacancies migrating out of the tunnels due to sintering. Turnbull and Tucker (Reference 10) have considered tunnel formation and sintering in detail. They found that the sintering flux or the flux of vacancies out of the tunnel surrounding one grain face is given by (Reference 10)

$$J = \frac{12\pi \gamma \delta' D_{gb} (b^{-1} + R_b^{-1})}{kT \left(1 + \frac{b D_{gb}}{2 R_b D_s} \right)} \quad , \tag{135}$$

where

D_{gb} = self-diffusion coefficient within a distance δ' of the grain boundary
b = tunnel radius
R_b = grain face radius given by Equation (64)
D_s = surface self-diffusion coefficient.

The total vacancy flux out of the tunnels per unit volume is given by

$$J_s = \frac{J}{2\pi R_g R_b^2} , \tag{136}$$

where R_g is the grain radius.

The total number of gas atoms going out of the boundary into the edge tunnels per unit volume per unit time is

$$\frac{\dot{a}_e}{\lambda R_g R_b} , \tag{137}$$

where $\dot{a}_e$ is the gas atom production rate in atom fraction per unit length of edge. The total number of gas bubbles per unit volume per unit time going from the boundary to the edge tunnels is given by

$$\frac{\dot{a}_e}{\lambda R_g R_b <n_b>} , \tag{138}$$

where $<n_b>$ is the average number of gas atoms in a grain boundary bubble given by Equation (62), (73), (88), or (96) depending on the operating conditions. The bubble radius is given by substituting the appropriate value of $<n_b>$ into either Equation (55) or (80). The total number of vacancies arriving at the tunnels per unit time and volume is given by multiplying the number of bubbles arriving, Equation (138), by $\alpha <r_b>^3$, where α is given by Equation (51), and dividing by the atomic volume, Ω. The number of vacancies arriving per unit volume and unit time is given by

$$J_a = \frac{\dot{a}_e}{\lambda R_g R_b <n_b>} \frac{\alpha <r_b>^3}{\Omega} . \tag{139}$$

The swelling due to tunnel formation is therefore

$$\left.\frac{\Delta V}{V}\right|_T = (J_a - J_s)\Omega . \tag{140}$$

If J_s is greater than J_a, then the tunnel network shrinks to the 5-percent volume size. At 5-percent volume the tunnels pinch off and form gas-free pores at the grain corners, maintaining the 5-percent volume. These pores heal just as the initial fabricated porosity healed, as discussed in Section II.K. In this work it will be assumed that once the tunnel network forms, it remains stable even if $J_s > J_a$; the tunnels simply do not grow.

The total fraction of gas released, f, is given by

$$f = \frac{\int_0^t (0.3 \text{ or } 0.34)\, \dot{i}\ (t')dt' - <C> N_0 - <C_b> \frac{3}{2 R_g \lambda^2}}{\int_0^t (0.3 \text{ or } 0.34)\, \dot{i}\ (t')dt'} \tag{141}$$

G. Temperature Gradients

In the case of the intragranular bubbles, spherical symmetry was used. In the presence of a temperature gradient the spherical symmetry is destroyed. In order to maintain the spherical symmetry, some assumptions have to be made. As stated in Reference 11, in the presence of a temperature gradient a gas bubble moves with a drift velocity given by

$$v = \frac{DF}{kT} , \tag{142}$$

where F is the force on the bubble due to the temperature gradient and is given in Reference 11 by

$$F = \frac{4\pi r^3 Q^* \nabla T}{3\Omega T} , \tag{143}$$

where Q^* is the heat of transport and is a function of the transport function of the bubble, and ∇T is the temperature gradient. If a bubble is placed in the center of a grain, then it will migrate out of the grain in time t, given by

$$t = \frac{R_g}{v} , \tag{144}$$

where R_g is the grain radius.

If a bubble is placed in the center of a grain in the absence of a temperature gradient, the time it takes to migrate out is given by

$$t = \frac{R_g^2}{6D} . \tag{145}$$

From Reference 7, an effective diffusion coefficient is defined by equating Equations (144) and (145) to obtain

$$D_{eff} = \frac{R_g v}{6} = \frac{R_g DF}{6\,kT} . \tag{146}$$

The diffusion coefficient used in Equation (22) is the sum of D and D_{eff}. If the temperature gradient is

zero, then D_{eff} is zero and normal diffusion holds. If $D_{eff} >> D$, then Equation (146) moves the gas out of the grains in approximately the same time as Equation (144) would predict.

The effect of temperature gradients on grain boundary bubbles has not been considered. Section II.H shows that the swelling due to grain boundary bubbles and the gas collected by the grain boundary bubbles is typically very small and hence relatively unimportant. Including the effect of a temperature gradient would reduce the gas on the grain boundaries even more; thus, the effect of the temperature gradient on the grain boundary gas is negligible.

H. Intragranular Densification

This section deals with the densification of fabricated pores which are found in the fuel at the beginning of the reactor operation.

When a uranium atom fissions, two highly energetic fission fragments are produced. These fission fragments lose energy first by ionizing the lattice atoms and then by knocking the lattice atoms out of the lattice sites. The regions of displaced atoms, or damage cascades, consist of vacancy clusters surrounded by isolated interstitials and a few isolated vacancies. At the relatively high temperatures of interest, microannealing takes place and the vacancy clusters can agglomerate and collapse into vacancy dislocation loops. It will be assumed here that one loop is formed for each fission fragment path. The cluster configuration has a very small effect on the point defect behavior because of the low density of the clusters. A large fraction of the interstitials migrate back to the damage cascade from which they originated. It will be assumed here that 10 percent of the interstitials created escape the damage cascade and become free to migrate through the lattice. In the swelling model, it is assumed that 1.0×10^5 lattice atoms are displaced per fission event. The number of interstitials assumed to escape the damage cascade is 10^4. In Reference 12, the number of vacancies escaping the two damage cascades per fission event is given by

$$\xi' = 10^4 - 2\frac{\pi r_d^2 b'}{\Omega} , \qquad (147)$$

where

r_d = radius of the collapsed vacancy loop
b' = Burgers vector of the loop
Ω = atomic volume.

The 2 in Equation (147) comes from the assumption that two damage cascades result from a fission event. In this work, the two cascades are treated as being of equal size.

The point defects, once created, can migrate to and be absorbed at dislocations, fabricated pores (henceforth called pores), damage cascades (treated as loops), grain or subgrain boundaries, and fission gas bubbles (neither treated as nor called pores). The point defects can also be destroyed by mutual recombination. The net absorption of interstitials at pores leads to densification, which is described by the MacEwen and Hastings (Reference 13) model. The calculation of the net arrival rate of interstitials to pores is the main concern here. Vacancy knockout by fission fragments will be discussed later.

From Reference 14, the loss rate of vacancies to dislocations is equal to

$$\frac{2\pi \rho' D_v}{\ln(r_1/b')} (C_v - C_o) ,$$

where

ρ' = dislocation density
D_v = vacancy diffusion coefficient
C_v = average vacancy concentration far from the dislocation
C_o = thermal equilibrium vacancy concentration
$r_1 (= 1/\sqrt{\pi\rho'})$ = half the distance between dislocations.

The dislocation density as a function of temperature has been given by Warner and Nichols (Reference 15) as

$$\rho' = \exp(-2.07 \times 10^{-3} (T - 273) + 21.82) , \qquad (148)$$

where T is the absolute temperature and the dislocation density is in units of cm^{-2}.

The loss rate of vacancies to pores is given in Reference 14 by

$$4\pi r_p N_p D_v \left\{ C_v - C_o \exp\left[\frac{\Omega}{kT} \left(\frac{2\gamma}{r_p} + P - P_g \right) \right] \right\} , \qquad (149)$$

where

r_p = pore radius (for simplicity only one pore size is considered)
N_p = number of pores per unit volume
k = Boltzmann's constant
γ = surface tension of the pore
P = externally applied hydrostatic pressure
P_g = pressure due to any fission gas that has accumulated in the pore.

The loss rate of vacancies to damage cascades is given in Reference 14 by

$$4\pi^2 r_d N_d D_v \left\{ C_v - C_o \exp\left[- \frac{\mu b \Omega \ln(32 r_d/b')}{4\pi(1-\nu) r_d kT} \right] \right\} \Big/ \ln(8r_d/b') , \quad (150)$$

where

r_d = damage cascade radius
N_d = number of cascades per unit volume
μ = shear modulus
ν = Poisson's constant.

From Reference 16, the loss rate of vacancies to grain or subgrain boundaries is given by

$$\frac{3 k_v D_v}{R_g} (C_v - C_o) , \quad (151)$$

where R_g is the radius of the grain or subgrain and k_v is given (Reference 16) by

$$k_v = \left[\frac{2\pi\rho'}{\ln(r_1/b')} + 4\pi(r_p N_p + r_d N_d) \right]^{1/2} . \quad (152)$$

The loss rate through recombination with interstitials is given in Reference 14 by

$$\frac{5040(D_i + D_v)}{\lambda^2} C_v C_i , \quad (153)$$

where C_i and D_i are the interstitial concentration and diffusion coefficient, respectively, and λ is the atomic jump distance.

The loss rate of vacancies to gas bubbles is difficult to calculate because the arrival of vacancies affects the energy of the gas. However, in-pile densification of intragranular pores is usually finished by a depletion of 1-2 $\times 10^{20}$ fissions/cm^3 and it is not necessary to calculate densification over a range of fission densities higher than this value. Up to this depletion and at temperatures below approximately 900°C, fission gas remains as isolated gas atoms and is not in bubbles. Isolated gas atoms would behave as any other impurity atom and would serve as trapping sites only and not as sink sites for point defects. Large gas bubbles may serve as sink sites. An interstitial would still be necessary to annihilate a vacancy. It is assumed that recombination at a trap site is included in the term given by Equation (153). At temperatures above 900°C, the vacancy concentration is approximately C_o so loss to large bubbles does not affect the vacancy concentration. Thus, the vacancy absorption at bubbles containing fission gas is not calculated (negligible effect) for this application.

By the use of Equations (148), (149), (150), (151), and (153), it can be shown that the rate of change in the vacancy concentration is given (Reference 12) by

$$\begin{aligned} \frac{dC_v}{dt} = {} & \dot{f}\,\Omega\,\xi - \frac{2\pi\rho' D_v}{\ln(r_1/b')} (C_v - C_o) \\ & + 4\pi r_p N_p D_v \left\{ C_o \exp\left[\frac{\Omega}{kT} \left(\frac{2\gamma}{r_p} + P - P_g \right) \right] - C_v \right\} \\ & + 4\pi^2 r_d N_d D_v \left\{ C_o \exp\left(+ \frac{\mu b' \Omega \ln(32 r_d/b')}{4\pi(1-\nu) r_d kT} \right) - C_v \right\} \Big/ \ln\frac{8r_d}{b'} \\ & - \frac{5040(D_i + D_v)}{\lambda^2} C_v C_i \\ & - \frac{3 k_v D_v}{R_g} (C_v - C_o) , \end{aligned} \quad (154)$$

where $\dot{f}$ is the fission rate.

An equation similar to Equation (154) exists for interstitials. It is given in Reference 12 by

$$\begin{aligned} \frac{dC_i}{dt} = {} & \dot{f}\,\Omega\,10^4 - \frac{2\pi D_i C_i \rho'}{\ln(r_1/(b' + \Delta R))} \\ & - 4\pi r_p N_p D_i C_i - 4\pi^2 r_d N_d D_i C_i \Big/ \ln\left(\frac{8r_d}{b'}\right) \\ & - \frac{5040(D_i + D_v) C_v C_i}{\lambda^2} \\ & - \frac{3 k_i D_i C_i}{R_g} , \end{aligned} \quad (155)$$

where from References 17 and 18,

$$\Delta R = 0.07\, b'\, \lambda^3\, \mu\, \epsilon / kT , \quad (156)$$

where ϵ is the size misfit parameter of an interstitial in the lattice, and from Reference 16

$$k_i = \left[\frac{2\pi\rho'}{\ln(r_1/(b' + \Delta R))} + 4\pi(r_p N_p + r_d N_d) \right]^{1/2} . \quad (157)$$

I. Damage Cascades

A simple and reasonable assumption, as was made in the case of depleted zones in Zircaloy in Reference 14, is that there is only one size of damage cascade. The size would be the average size of

the cascade over its lifespan. The number of vacancies in such a cascade would be approximately half the number there were when the cascade was created. If it is assumed that all of the vacancies are in the cascade cluster at creation (approximately 0.5×10^4), then the average cascade would have approximately half that number at midlife or approximately 2500 vacancies. The effective isolated vacancy generation rate would then be $\xi = 5000$, and the cascade loop radius would be given by

$$r_d = \left(\frac{2500\,\Omega}{\pi b'}\right)^{1/2} \tag{158}$$

A cascade increases in size by absorbing vacancies. It decreases in size by absorbing interstitials and emitting vacancies. The net flux of interstitials to damage cascades per unit volume is given in Reference 12 by

$$J = 4\pi^2 r_d N_d N_o \Big/ \ln(8r_d/b') \left\{ D_i C_i + D_v \left[C_o \exp\left(- \frac{\mu b' \Omega \ln(32\, r_d/b')}{4\pi(1-\nu) r_d kT} \right) - C_v \right] \right\}, \tag{159}$$

where N_o is the number of lattice sites per unit volume.

The total net number of interstitials to fill all cascades is given by

$$\frac{\pi r_d^2 b' N_d}{\Omega} \tag{160}$$

The rate (number per second) at which cascades are filled is Equation (160) divided by Equation (159). The change in the number of cascades due to filling is the number of cascades divided by the rate at which they are filled. The rate at which cascades are created is $2\dot{f}$. From Reference 12, the rate of change in the number of cascades is given by

$$\frac{dN_d}{dt} = 2\dot{f} - \frac{N_d 4\pi}{r_d b' \ln(8r_d/b')} \left\{ D_i C_i + D_v \left[C_o \exp\left(- \frac{\mu b' \Omega \ln(32\, r_d/b')}{4\pi(1-\nu) r_d kT} \right) - C_v \right] \right\}. \tag{161}$$

J. Pore Behavior

Pores, as in the case of damage cascades, grow by absorbing vacancies; they shrink by absorbing interstitials and emitting vacancies. Letting n_p be the number of interstitials it takes to fill a pore, then the net flux of interstitials to the pore is given (Reference 12) by

$$\frac{dn_p}{dt} = 4\pi r_p N_o D_i C_i + 4\pi r_p N_o D_v \left\{ C_o \exp\left[\frac{\Omega}{kT}\left(\frac{2\gamma}{r_p} + P - P_g\right)\right] - C_v \right\}. \tag{162}$$

The volume of a pore, V_p, is related to the pore radius and the number of interstitials to fill the pore by the equation

$$V_p = \frac{4}{3}\pi r_p^3 = n_p \Omega$$

so that

$$\frac{dV_p}{dt} = \Omega \frac{dn_p}{dt} = 4\pi r_p^2 \frac{dr_p}{dt} \tag{163}$$

Therefore, by the use of Equations (162) and (163), the following equation is obtained:

$$\frac{dr_p}{dt} = -\frac{1}{r_p}\left[D_i C_i + D_v \left\{ C_o \exp\left[\frac{\Omega}{kT}\left(\frac{2\gamma}{r_p} + P - P_g\right)\right] - C_v \right\} \right]. \tag{164}$$

The pressure of the gas in the pore, P_g, is calculated from a simplified van der Waals gas law and is given by

$$P_g = \frac{n_g kT}{\left(\frac{4}{3}\pi r_p^3 - \beta n_g\right)}, \tag{165}$$

where β is van der Waals gas constant and n_g is the number of gas atoms in the pore. The change in the number of gas atoms in a pore with respect to time is given in Reference 12 by

$$\frac{dn_g}{dt} = 4\pi r_p D C N_o - \frac{n_g}{\tau}, \tag{166}$$

where D is the fission gas diffusion coefficient, and C is the fission gas concentration which is a function of temperature, depletion, grain size, etc. D and C are the same as those used in Equation (22).

The first term on the right-hand side of Equation (166) is the rate at which gas migrates to the pore, and the second term is the rate at which it is knocked out by fission fragments passing through the pore.

Very early, C is essentially zero; therefore, n_g and P_g are essentially zero and hence unimportant

as far as calculating the change in the pore radius with respect to time. After a time τ (approximately 7 hours), Equation (166) reaches a steady state value; therefore, for the work reported herein, it is assumed that the gas is always in steady state in the pores so that

$$n_g = 4\pi r_p D C N_o \tau \quad . \qquad (167)$$

At this point, there are four equations [Equations (154), (155), (161), and (164)] in four unknowns (C_v, C_i, N_d, and r_p) which can be solved simultaneously. These equations must be combined with the swelling and gas release model to obtain C and D. Since the interstitials diffuse very rapidly at the temperature of interest here, it is assumed that they are in steady-state equilibrium; thus dC_i/dt can be set equal to zero. With $dC_i/dt = 0$, Equations (154), (155), (161), and (164) were solved with the initial conditions that $C_v = C_o$, $N_d = 0$, and $r_p = 10^{-4}$ cm. It was found that, with the large production rate of interstitials (10^{17}/cm^3 second with a fission rate 10^{13} fissions/cm^3 second) and with the somewhat smaller production rate of vacancies, the interstitials impose a steady-state concentration on the vacancies far sooner than if the vacancies approached steady state through their own diffusion. The vacancies reached steady state in less than a second at temperatures down to 200°C. Because of the rapid approach of vacancies to steady state, dC_v/dt can also be set equal to zero.

Equations (154), (155), (161), and (164) were solved assuming both dC_v/dt and dC_i/dt equal zero.

Stehle and Assmann (Reference 19) have pointed out that when a fission fragment passes through a pore, the resulting disruption can "knock" vacancies from the pore to the lattice. Some of the vacancies diffuse away from the pore to other sinks and the pore shrinks. The exact details of such a knocking process are most likely very complicated and no attempt will be made here to discuss them. What is needed is an estimate of the number of times per second a pore is hit by a fission fragment and the number of vacancies that escape per hit (this will be called η). The number of hits per second is equal to the number of fission fragments produced per second, times the volume around each pore through which the fragment can travel and remove vacancies from the pore, times the number of pores. The number of fission fragments produced per second is $2\dot{f}$ and the total volume in which they can cause vacancies to leave the pore is $4\pi r_p^2 N_p \lambda'$, where λ' is the "viable" length of the fission fragment path. Immediately after a fragment is created, its energy is too great to cause displacements; however, during approximately the last 10 percent of the path length the energy is low enough to cause displacements. This is the "viable" path length. Since the total path length is 10μ, the "viable" path length is approximately 1μ.

The probability that a particular pore is hit by a fragment is

$$2\dot{f}\ 4\pi r_p^2 \lambda' \quad . \qquad (168)$$

If the number of vacancies knocked out of a pore per collision is η (assumed to be approximately 100), then the number of vacancies knocked out of the pore per second is

$$2\dot{f}\ 4\pi r_p^2 \lambda' \eta \quad . \qquad (169)$$

It is an easy matter to show that the change in the pore radius with respect to time is given by

$$\frac{dr_p}{dt} = -\Omega\, 2\dot{f}\ \lambda' \eta \quad . \qquad (170)$$

The total change in the pore radius with respect to time is now given by adding Equation (170) to Equation (164). The vacancy production rate from the pores is given by

$$\frac{dC_v}{dt} = 8\pi\ \dot{f}\ r_p^2 \lambda' \eta N_p \Omega \quad . \qquad (171)$$

The vacancy production rate given by Equation (171) must now be added to Equation (154) to get the total change in the vacancy concentration with respect to time.

K. Densification of Intergranular Porosity

There are two types of intergranular porosity which are considered in this report: (1) interconnected, which has already been discussed, and (2) grain corner. Pores which occur between two grains will be assumed to behave as those in the corners. This is a good assumption since most intergranular porosity left over from densification occurs at the grain corners. Also, many of these pores are on the order of the grain size and hence must be in the corners.

The pores grow by absorbing vacancies and shrink by emitting vacancies and absorbing interstitials. To the point defects at the grain interior, the corner pores appear as part of the boundary. The interstitial concentration at the pore is zero and the vacancy concentration is given by

$$C_o \exp\left[\frac{\Omega}{kT}\left(\frac{2\gamma}{r_p'} + P - P_g'\right)\right] , \qquad (172)$$

as opposed to C_o as it is elsewhere on the boundary. In Equation (172), r'_p is the corner pore radius and P'_g is the pressure due to the fission gas that has migrated to the pores.

Using Equation (172), the rate at which vacancies diffuse from the grain interior to the pores can be calculated. It is assumed that the presence of a pore does not change the vacancy or interstitial concentration in the grains. It can be shown that the vacancy production rate due to fissioning is about 100 times larger than that due to vacancy knockout from the pores.

The net flux of vacancies into a pore per unit area of pore is given by

$$K_v D_v N_o \left\{ C_v - C_o \exp\left[\frac{\Omega}{kT}\left(\frac{2\gamma}{r'_p} + P - P'_g\right)\right]\right\} . \quad (173)$$

The net flux of vacancies into the pore is given by

$$4\pi r'^2_p N_o k_v D_v \left\{ C_v - C_o \exp\left[\frac{\Omega}{kT}\left(\frac{2\gamma}{r'_p} + P - P_g\right)\right]\right\} . \quad (174)$$

In a similar fashion the net flux of interstitials into the pore from the grain interior is given by

$$4\pi r'^2_p N_o k_i D_i C_i . \quad (175)$$

The net flux of vacancies into a pore from the grain interior is given by

$$J_1 = -4\pi r'^2_p N_o \left[k_i D_i C_i - k_v D_v \left\{C_v - C_o \exp\left[\frac{\Omega}{kT}\left(\frac{2\gamma}{r'_p} + P - P_g\right)\right]\right\}\right] . \quad (176)$$

Vacancies can also migrate out of the pores along the grain boundaries. The vacancy flux per unit length of boundary in contact with a pore is given by

$$j = D_{V_g} \frac{\Delta C}{\Delta x} , \quad (177)$$

where

$$\Delta C = C_o \exp\left[\frac{\Omega}{kT}\left(\frac{2\gamma}{r'_p} + P - P'_g\right)\right] - C_o , \quad (178)$$

and Δx is taken as the radius of a grain face, R_b; D_{V_g} is the vacancy diffusion coefficient in a region δ' thick along the grain boundaries. D_{V_g} is related to the grain boundary self-diffusion coefficient by the equation

$$D_{gb} = D_{V_g} C_o . \quad (179)$$

The number of vacancies that migrate out of the pore per second per unit length of boundary intersecting the pore is given by

$$j = \frac{N_o D_{V_g} \delta' \left\{C_o \exp\left[\frac{\Omega}{kT}\left(\frac{2\gamma}{r'_p} + P - P'_g\right)\right] - C_o\right\}}{R_b} \quad (180)$$

If it is assumed that the pore is spherical and is at the corner of four grains, then it can be shown that the total boundary line length intersecting the pore is $11.46\, r'_p$.

The net flux of vacancies out of the pore due to diffusion along the grain boundary per pore is given by

$$J_2 = \frac{-11.46 r_p N_o D_{gb} \delta' \left\{\exp\left[\frac{\Omega}{kT}\left(\frac{2\gamma}{r'_p} + P - P_g\right)\right] - 1\right\}}{R_b} . \quad (181)$$

Vacancies are also brought into the pores from gas bubbles migrating to the pores along the grain boundary edges. The rate at which gas atoms reach the pores is the same as the rate at which they migrate into the corner bubbles. Define $\dot{a}_c$ as the number of gas atoms that migrate to the corner bubbles per unit time. The number of vacancies arriving per gas atom is approximately β/Ω. The number of vacancies arriving at the pore per second is given by

$$J_3 = \frac{\beta}{\Omega} \dot{a}_c . \quad (182)$$

The change in the radius with respect to time due to point defect diffusion is given by

$$\frac{dr'_p}{dt} = \frac{\Omega J}{4\pi r'^2_p} , \quad (183)$$

where J is the net number of vacancies arriving at the pore per unit time and is the sum of J_1, J_2, and J_3. From Equation (170), the change in the pore radius due to vacancy knockout by fission fragments can be calculated. It was previously stated that the number of grain corners per cm^3 is $0.695/(R_g^2 R_b)$. If there are N'_p grain boundary pores, then there can only be $0.695/(R_g^2 R_b) - N'_p$ grain corner bubbles. The corner swelling is then given by

$$\left.\frac{\Delta V}{V}\right|_c = \frac{4}{3}\pi r_c^3 \left(\frac{0.695}{R_g^2 R_b} - N'_p\right) + \frac{4}{3}\pi r'^3_c N'_p . \quad (184)$$

When

$$\left.\frac{\Delta V}{V}\right|_c + \left.\frac{\Delta V}{V}\right|_e$$

is greater than 5 percent, then tunnels form. If the initial porosity due to corner pores is greater than 5 percent, then tunnels form immediately. When r'_p is less than r_c, corner pores should be treated as corner bubbles. The amount of gas in a corner pore is the same as that in a corner bubble as given by Equation (132). The gas pressure in a corner pore is given by

$$P'_g = \frac{n'_c\, kT}{\left(\frac{4}{3}\pi\, r'^3_p - \beta\, n_c\right)} \quad (185)$$

III. COMPARISONS WITH EXPERIMENTAL DATA

Theoretical predictions of gas release, swelling, and densification in both ThO_2 and UO_2 were obtained using the constants given in the Nomenclature. Figure 1 compares predicted gas release for UO_2 with data of Lewis (Reference 20). The fission rate is 10^{13} fissions/cm^3 second. The temperature gradient is assumed to be 1000°C/cm and the grain radius is assumed to be 10^{-3} cm. To make the predictions, the radius of the fuel rods was divided into three equal lengths and the average temperature in each of the three regions was calculated assuming a fuel surface temperature of 400°C. In most cases reasonable agreement is obtained between predictions and data.

Figure 2 shows the fission-gas release data of Zimmermann for UO_2-20% PuO_2 (Reference 21). The fission rate is 10^{14} fissions/cm^3 second. The maximum clad temperatures were between 443 and 690°C. Zimmermann provided average fuel temperatures. Using these temperatures and the clad surface temperatures, temperature profiles were constructed using assumed parabolic temperature profiles. A temperature gradient of 1000°C/cm and a grain diameter between 1 and 2μm were used for the calculation. Three different sets of theoretical curves were generated using average fuel temperatures of 1000, 1250, and 1500°C. In constructing Figure 2, the same physical constants as those used for UO_2 were employed.

The theoretical predictions were also compared with the data of Hilbert et al. (Reference 22) for UO_2; the results are shown in Table 1 and in Figure 3. The initial grain size was 10μm and the grains were equiaxed. The final grain size varied from 20μm-diameter equiaxed grains to columnar grains 50μm diameter by approximately 800μm long at the highest temperatures. At the higher temperatures gas release was nearly 100 percent and swelling due to gas was approximately zero; consequently, results are presented assuming 10μm-diameter and 50μm-diameter grains and assuming that these limits adequately predict the limits of the observed conditions. Both theory and experiment show a decrease in swelling with temperature. It should be pointed out that the Hilbert et al. (Reference 22) temperatures are higher than the present model can accurately accommodate, since no allowance was made in the model for the columnar grain formation which occurred in their higher temperature regions.

Figure 4 shows the gas-release data of Bellamy and Rich (Reference 23) as a function of burnup. The UO_2 specimens were irradiated at a fission rate of about 2×10^{13} fissions/cm^3 second and had a grain radius of 7.5μm. The center line temperatures were, on the average, about 1200°C and the fuel surface temperatures were approximately 600°C. Fuel center line temperatures of a few specific specimens are shown in Figure 4. Also shown are the model predictions assuming center line temperatures of 800, 1200, and 1400°C with a surface temperature of 600°C.

Comparisons have been made between the model and the data of Freshley et al. (Reference 24). The results are shown in Table 2. The pellets were 0.92 cm diameter. The fuel surface temperature was taken as 550°C when the center line temperature exceeded 550°C. In making the predictions, it was assumed that the small pores were intragranular and that the large pores were on the gain boundaries. The predicted density changes versus the observed density changes are plotted in Figure 5. The majority of the predictions are within 2 percent of the observed changes; however, in some cases the predictions result in a positive $\Delta\rho$ while the measurements indicate some swelling. On the whole, the model predicts a little more densification than that observed by Freshley et al. (Reference 24).

Comparisons were also made between the model and the data of Banks (Reference 25). The results are shown in Table 3. Table 4 shows the initial porosity for each of the specimen types. The small pores are assumed to be 2μm diameter and the large pores 10μm diameter. The pellets were 1.45 cm diameter. A fuel surface temperature of 500°C was assumed when the center line temperatures exceeded 500°C. The predicted volume increase above 100 percent dense fuel versus the observed volume increase for Banks' specimens are shown in Figure 6. Almost all of the predictions are within 2 percent of the observed results.

The model was also compared with densification data of Ross (Reference 26). Ross irradiated UO_2 at 200°C and observed that pores up to 0.5μm diameter were removed after irradiation of 3×10^{19} fissions/cm^3. The model here predicts complete densification by depletion of 1×10^{19} fissions/cm^3. Ross also observed that most

0.3μm-diameter pores were removed by a burnup of 3.0×10^{18} fissions/cm^3. The model predicts complete densification by 3.2×10^{18} fissions/cm^3. The model is, therefore, in good agreement with the Ross data.

A thoria specimen was irradiated at a center line temperature of 1470°C and with a surface temperature of 570°C to a depletion of 3.5×10^{20} fissions/cm^3*. The initial density was 93 percent. The initial grain size was about 4.5×10^{-3} cm. The initial average pore size was about 2μm diameter. Under these conditions, the volume was observed to decrease 2.9 percent. The model predicts a decrease of 4 percent. Under the above conditions, it was observed that 1 percent of the fission gas generated was released. The model predicts 2.5 percent. The model also predicts complete closure of the fabricated pores.

Another thoria rod, 81-90**, was fissioned to a depletion of 2×10^{19} fissions/cm^3 at a fission rate of about 3.4×10^{12} fissions/cm^3 second. The center line temperature of the fuel was about 427°C and the surface temperature was about 367°C. The grain size was 7μm, and the initial porosity was 2.6 percent. The final porosity measured experimentally was 1.4 percent; the model predicts 2 percent. There was no gas release observed experimentally or predicted by the model. It was assumed that 0.26 percent of the initial porosity was in the form of 2μm-diameter pores and that 2.34 percent of the initial porosity was in the form of 6μm-diameter pores. The latter pores were assumed to be on the grain boundaries. In the case of the Waldman specimen, the model predicts slightly more densification than that observed and in the case of the Spahr specimen the model predicts less densification that that observed.

IV. SUMMARY AND CONCLUSIONS

A model was developed to predict the migratory behavior of fission-induced gas in oxide fuels. The model can predict gas bubble size and density in the grain interior and on grain boundaries, grain edges, and corners. The model includes resolution effects and restricted bubble motion, both random and along thermal gradients. The resulting swelling is predicted. Gas release from tunnels along the grain edges is also calculated.

The model was also developed to predict intragranular and intergranular densification. The model treats both densification due to thermal diffusion of point defects and pore destruction due to fission fragment passage through the pores.

Comparisons were made between the gas release data of Lewis (Reference 20), Zimmermann (Reference 21), Hilbert et al. (Reference 22), Bellamy and Rich (Reference 23) and theory with good agreement. Comparisons were also made between theory and the swelling data of Hilbert et al. (Reference 22), Freshley et al. (Reference 24), Banks (Reference 25), Ross (Reference 26), Waldman, and Spahr with good agreement.

V. ACKNOWLEDGMENTS

The author wishes to express his appreciation to E. Duncombe, E. A. Zanoni, and F. A. Nichols for their many helpful comments; also to L. A. Waldman and G. L. Spahr for making ThO_2 experimental data available.

VI. REFERENCES

1. C. C. Dollins and H. Ocken, "A Fission Gas Swelling Model Incorporating Re-solution Effects," *Nucl. Appl. and Tech. 9*, 141 (1970) and WAPD-TM-962, July 1971.
2. A. C. Damask and G. J. Dienes, Point Defects in Metals, p. 82, Gordon and Breach, New York, 1963.
3. C. C. Dollins, "Fission Gas Swelling and Long-Range Migration at Low Temperatures," *J. Nucl. Mater., 49*, 10 (1973) and WAPD-TM-1124, January 1974.
4. B. J. Buescher and R. O. Meyer, "Thermal-Gradient Migration of Helium Bubbles in Uranium Dioxide," *J. Nucl. Mater., 48*, 143 (1973).
5. D. Davies and G. Long, "The Emission of Xenon-133 from Lightly Irradiated Uranium Dioxide Spheroids and Powders," Rpt. U. K. Atomic Energy Auth., AERE-R-4347, (1963).
6. R. S. Nelson, "The Stability of Gas Bubbles in an Irradiation Environment," *J. Nucl. Mater., 31*, 153 (1969).
7. C. C. Dollins and F. A. Nichols, "Swelling and Gas Release in UO_2 at Low and Intermediate Temperatures," *J. Nucl. Mater., 60*, 138 (1976).
8. A. Dvoretzky and P. Erdos, "Some Problems on Random Walk in Space," in Proc. 2nd Berkeley Symposium on Mathematical Statistics and Probability, ed. by J. Newyman, University of Calif. Press, Berkeley, p. 353, 1951.
9. G. H. Vineyard, "The Number of Distinct Sites Visited in a Random Walk on a Lattice," *J. of Mathematical Phys., 4*, 1191 (1963).
10. J. A. Turnbull and M. O. Tucker, "Swelling in UO_2 Under Conditions of Gas Release," *Phil. Mag., 30*, 47 (1974).
11. F. A. Nichols, "On the Diffusional Mobilities of Particles, Pores, and Loops," *Acta Met., 20*, 207 (1972).

*Information obtained from L. A. Waldman, Bettis Atomic Power Laboratory, October, 1976.
**Information obtained from G. L. Spahr, Bettis Atomic Power Laboratory, January, 1977.

12. C. C. Dollins and F. A. Nichols, "In-pile Intragranular Densification of Oxide Fuels (AWBA Development Program)," WAPD-TM-1293, October 1977.
13. S. R. MacEwen and I. J. Hastings, "A Model for In-Reactor Densification of UO_2," *Phil. Mag., 31,* 135 (1975).
14. C. C. Dollins, "In-pile Dimensional Changes in Neutron Irradiated Zirconium Base Alloys," *J. Nucl. Mater., 59,* 61 (1975).
15. H. R. Warner and F. A. Nichols, "A Statistical Fuel Swelling and Fission Gas Release Model," *Nucl. Appl. and Tech., 9,* 148 (1970) and WAPD-TM-942, September 1970.
16. A. D. Brailsford and R. Bullough, "Swelling of Irradiated Materials," in Physical Metallurgy of Reactor Fuel Elements, p. 148, The Metals Society, 1975.
17. F. S. Ham, "Stress-Assisted Precipitation on Dislocations," *J. of Appl. Physics, 30,* 915 (1959).
18. S. D. Harkness and C. Y. Li, "A Study of Void Formation in Fast Neutron-Irradiated Metals," *Met. Trans., 2,* 1457 (1971).
19. H. Stehle and H. Assmann, "The Dependence of In-Reactor UO_2 Densification on Temperature and Microstructure," *J. Nucl. Mater., 52,* 303 (1974).
20. W. B. Lewis, "Engineering for the Fission Gas in UO_2 Fuel," *Nucl. App., 2,* 171 (1966).
21. H. Zimmermann, "Fission Gas Behavior in Oxide Fuel Elements of Fast Breeder Reactors," *Nucl. Tech., 28,* 127 (1976).
22. R. F. Hilbert, V. W. Storhok, W. Chubb, and D. L. Keller, "Mechanisms of Swelling and Gas Release in Uranium Dioxide," *J. Nucl., Mater., 38,* 26 (1971).
23. R. G. Bellamy and J. B. Rich, "Grain-Boundary Gas Release and Swelling in High Burnup Uranium Dioxide," *J. Nucl. Mater., 33,* 64 (1969).
24. M. D. Freshley, D. W. Brite, J. L. Daniel, and P. E. Hart, "Irradiation-Induced Densification of UO_2 Pellet Fuel," *J. Nucl. Mater., 62,* 138 (1976).
25. D. A. Banks, "Some Observations of Density and Porosity Changes in UO_2 Fuel Irradiated in Water-Cooled Reactors," *J. of Nucl. Mater., 54,* 97 (1974).
26. A. M. Ross, "Irradiation Behavior of Fission-Gas Bubbles and Sintering Pores in UO_2," *J. Nucl. Mater., 30,* 134 (1969).

TABLE 1. SWELLING AND GAS RELEASE DATA OF HILBERT et al.

Burnup × 10^{-20} fissions/cm^3	Center Line Temperature, °C	Fuel Surface Temperature, °C	$\frac{\Delta V}{V}$, Swelling, %		Gas Release, %	
			Measured	Predicted	Measured	Predicted
2.3	2190	1825	5	5.5-6	90-100	97-99
1.7	1855	1475	10	5.6-9.2	90	94-95
2.25	2030	1620	5	5.8-7.9	90	96.8-98
2.45	2000	1630	—	5.9-8.3	90	97-98
1.85	2050	1490	8	5.7-7.3	80	96
1.75	1660	1310	10	5.6-9.4	75	71-87

TABLE 2. COMPARISONS BETWEEN MODEL AND DATA OF FRESHLEY et al.

Type 1 fuel, grain size = 3μm, small pore size = 0.4μm, small pore volume = 6.3%, large pore size = 2.0μm, large pore volume = 1.3% ± 0.2

Pin Location	Fission Rate (cm^{3}sec)$^{-1}$	Center Line Temperature, °C	Burnup MWd/MTM	Average $\Delta\rho$%	
				Measured	Predicted
A-85	3.4×10^{12}	310	224	0.48	1.9
A-86	3.2×10^{12}	300	214	0.66	
A-11	9.6×10^{12}	910	646	5.41	4.4
A-12	1.01×10^{13}	955	677	5.30	
A-49	1.29×10^{13}	1235	860	6.23	4.9
A-50	1.25×10^{13}	1200	839		
B-85	3.4×10^{12}	310	815	1.86	5.0
B-86	3.2×10^{12}	300	792	1.17	
B-11	9.6×10^{12}	910	2335	6.67	6.6
B-12	1.01×10^{13}	955	2462	5.88	
B-49	1.24×10^{13}	1190	2996	7.13	6.2
B-50	1.24×10^{13}	1190	2996	7.12	

TABLE 2 (Cont)

Type 2 fuel, grain size = 4μm, small pore size = 0.6μm, small pore volume = 6.8%, large pore size = 3.0μm, large pore volume 2.4 ± 0.4%

Pin Location	Fission Rate $(cm^3sec)^{-1}$	Center Line Temperature, °C	Burnup MWd/MTM	Average Δρ%	
				Measured	Predicted
A-72	6.6×10^{12}	610	437	0.96	2.7
A-73	6.3×10^{12}	580	417	0.82	
A-45	1.35×10^{13}	1295	895	5.22	4.4
B-72	6.4×10^{12}	600	1583	2.40	6.6
B-73	6.3×10^{12}	585	1520	1.71	
B-45	1.32×10^{13}	1265	3190	6.19	7.0
B-47	1.27×10^{13}	1220	3083	6.17	

Type 3 fuel, grain size = 14μm, small pore size = 1.2μm, small pore volume = 1.2%, large pore size = 1.5μm, large pore volume = 4.1 ± 0.4%

Pin Location	Fission Rate $(cm^3sec)^{-1}$	Center Line Temperature, °C	Burnup MWd/MTM	Average Δρ%	
				Measured	Predicted
A-77	5.2×10^{-12}	470	344	−0.47	1.5
A-79	4.7×10^{12}	425	318	−0.65	
A-55	1.16×10^{13}	1080	776	0.05	2.2
A-56	1.13×10^{13}	1050	755	0.16	
A-37	1.41×10^{13}	1325	943	0.82	2.2
A-38	1.41×10^{13}	1325	943	0.33	
B-78	4.9×10^{12}	440	1199	−0.45	3.3
B-79	4.9×10^{12}	440	1179	−0.46	
B-37	1.41×10^{13}	1320	3403	0.84	3.7
B-38	1.41×10^{13}	1320	3397	0.58	

TABLE 2 (Cont)

Type 4 fuel, grain size = 5μm, small pore size = 0.5μm, small pore volume = 6.3%, large pore size = 2.0μm, large pore volume = 0.6 ± 0.3%.

Pin Location	Fission Rate $(cm^3 sec)^{-1}$	Center Line Temperature, °C	Burnup MWd/MTM	Average $\Delta\rho$%	
				Measured	Predicted
A-69	7.7×10^{12}	675	505	2.29	3.1
A-70	7.0×10^{12}	640	474	1.99	
A-43	1.41×10^{13}	1325	937	5.08	4.2
A-44	1.38×10^{13}	1290	916	5.04	
B-81	4.3×10^{12}	380	1049	1.74	4.9
B-82	4.1×10^{12}	370	1005	1.63	
B-69	7.8×10^{12}	710	1884	4.21	6.2
B-70	7.3×10^{12}	670	1797	4.13	
B-43	1.36×10^{13}	1275	3290	5.25	5.3
B-44	1.35×10^{13}	1260	3253	5.18	

Type 5 fuel, grain size = 16μm, small pore size = 0.4μm, small pore volume = 1.5%, large pore size = 13μm, large pore volume = 7.2 ± 0.7%.

Pin Location	Fission Rate $(cm^3 sec)^{-1}$	Center Line Temperature, °C	Burnup MWd/MTM	Average $\Delta\rho$%	
				Measured	Predicted
A-1	6.1×10^{12}	550	406	−0.38	1.1
A-3	6.9×10^{12}	625	458	−0.33	
A-27	1.36×10^{13}	1270	906	0.08	1.6
A-28	1.36×10^{13}	1270	911	−0.06	
B-1	6.0×10^{12}	555	1433	−0.58	2.1
B-3	6.6×10^{12}	600	1583	−0.37	
B-27	1.32×10^{13}	1230	3210	−0.44	2.6
B-28	1.35×10^{13}	1260	3277	−0.27	

TABLE 2 (Cont)

Type 6 fuel, grain size = 22μm, small pore size = 0.6μm, small pore volume = 1.9%, large pore size = 9.0μm, large pore volume = 5.0 ± 0.4%.

Pin Location	Fission Rate $(cm^3sec)^{-1}$	Center Line Temperature, °C	Burnup MWd/MTM	Average Δρ%	
				Measured	Predicted
A-4	6.9×10^{12}	640	468	−0.46	1.2
A-6	8.0×10^{12}	725	526	−0.39	
A-30	1.39×10^{13}	1300	932	0.30	1.5
A-31	1.41×10^{13}	1325	937	−0.07	
B-4	6.9×10^{12}	625	1660	−0.42	2.5
B-6	7.7×10^{12}	695	1864	−0.42	
B-58	1.1×10^{13}	1020	2675	−0.04	2.5
B-60	9.9×10^{12}	910	2418	−0.24	
B-61	9.9×10^{12}	910	2398	0.00	
B-30	1.36×10^{13}	1275	3320	0.04	1.8
B-31	1.38×10^{13}	1290	3340	−0.10	

Type 7 fuel, grain size = 24μm, small pore size = 0.6μm, small pore volume = 1.8%, large pore size = 30μm, large pore volume = 5.7 ± 0.4%.

Pin Location	Fission Rate $(cm^3sec)^{-1}$	Center Line Temperature, °C	Burnup MWd/MTM	Average Δρ%	
				Measured	Predicted
A-66	8.3×10^{12}	750	552	−0.07	0.8
A-67	8.3×10^{12}	750	547	−0.20	
A-40	1.41×10^{13}	1325	943	0.26	1.2
A-41	1.42×10^{13}	1325	948	0.40	
B-88	2.8×10^{12}	250	685	−0.55	1.0
B-89	2.8×10^{12}	250	665	−0.73	
B-90	2.6×10^{12}	240	621	−0.73	
B-65	8.9×10^{12}	810	2141	−0.32	1.7
B-67	8.4×10^{12}	770	2034	−0.17	
B-40	1.39×10^{13}	1300	3360	0.48	0.7
B-41	1.36×10^{13}	1275	3297	−0.03	

TABLE 2 (Cont)

Type 8 fuel, grain size = 23μm, small pore size = 0.6μm, small pore volume = 1.5%, large pore size = 2.1μm, large pore volume = 1.3 ± 0.3%

Pin Location	Fission Rate $(cm^3sec)^{-1}$	Center Line Temperature, °C	Burnup MWd/MTM	Average $\Delta\rho$%	
				Measured	Predicted
A-74	6.1×10^{12}	535	406	−0.19	0.8
A-76	5.4×10^{12}	465	359	−0.27	
A-33	1.44×10^{13}	1320	958	0.23	1.3
A-34	1.45×10^{13}	1330	974	−0.11	
B-75	6.0×10^{12}	520	1433	−0.42	1.8
B-76	5.7×10^{12}	490	1369	−0.38	
B-33	1.39×10^{13}	1270	3360	0.00	1.3
B-34	1.41×10^{13}	1290	3427	−0.06	

Type 9 fuel, grain size = 29μm, small pore size = 0.6μm, small pore volume = 1.5%, large pore size = 2.1μm, large pore volume = 1.3 ± 0.3%.

Pin Location	Fission Rate $(cm^3sec)^{-1}$	Center Line Temperature, °C	Burnup MWd/MTM	Average $\Delta\rho$%	
				Measured	Predicted
A-7	8.7×10^{12}	770	578	−0.24	1.8
A-9	9.3×10^{12}	830	619	−0.17	
A-51	1.27×10^{13}	1150	844	0.20	1.9
A-53	1.24×10^{13}	1120	823	0.22	
B-7	8.3×10^{12}	730	2014	−0.10	3.4
B-9	9.2×10^{12}	815	2228	0.05	
B-52	1.21×10^{13}	1090	2946	0.03	3.3
B-53	1.21×10^{13}	1090	2946	0.16	

TABLE 3. COMPARISONS BETWEEN MODEL AND DATA OF BANKS

Cluster	Irradiation Time, EFPD	Burnup × 10^{20} fissions/cm^3	Center Line Temperature, °C	$\frac{\Delta V}{V}$, Swelling, %	
				Observed	Predicted
E11/2	660	0.88	460	3.19	2.7
		2.65	850	3.10	2.6
		3.82	1040	2.74	4.9
L09/2	385	0.51	480	2.83	2.3
		1.56	860	1.73	1.7
		2.58	1270	2.28	4.4
		3.12	1500	2.83	4.7
		3.26	1560	3.01	4.8
Q03/2	365	0.98	1090	1.64	2.9
		1.58	1370	3.38	4.4
		2.45	1712	3.74	4.7
		2.94	2160	6.2	6.0
		3.15	2170	5.75	6.3
L05/2	360	0.09	360	3.56	3.4
		0.09	360	3.56	
		0.18	390	3.65	3.7
		0.28	410	3.74	3.7
		0.37	460	3.74	3.7
		0.44	460	2.92	3.0
		0.49	500	3.56	2.9
		0.49	480	3.28	
		0.49	500	3.28	
L05/2	360	0.63	550	3.28	2.9
		0.68	560	3.38	2.8
		0.75	600	3.19	2.7
		0.86	620	3.10	2.7
		0.98	660	3.01	2.7
		1.07	700	3.28	2.6
		1.12	720	3.19	2.7
		1.37	1133	3.56	3.4
		2.28	1573	8.03	4.6
		2.75	1709	7.48	5.2
		3.03	1796	7.12	5.6
IFA29 Solid Pellets	420	3.05	1100	3.28	3.9
		3.33	1200	3.10	4.6
		3.68	1360	3.56	4.7
		4.40	1580	4.23	6.0
		4.98	1790	4.74	7.1
		5.43	2000	4.84	7.3
		5.79	2120	5.47	7.5
IFA29 Hollow Pellets	420	3.05	1090	2.92	2.9
		3.68	1200	3.47	4.8
		4.40	1380	6.57	5.1
		4.98	1730	7.48	7.1
		5.43	1910	7.57	7.6
		5.79	2220	7.20	7.5

TABLE 4. SPECIMEN TYPES

Cluster	Initial Porosity, %	Small Pore Density	Large Pore Density
E11/2	3.65	$1.55 \times 10^9/cm^3$	$5.73 \times 10^7/cm^3$
L09/2	2.92	$2.20 \times 10^9/cm^3$	$3.82 \times 10^7/cm^3$
Q03/2	3.19	$1.65 \times 10^9/cm^3$	$4.77 \times 10^7/cm^3$
L05/2	3.65	$1.55 \times 10^9/cm^3$	$5.73 \times 10^7/cm^3$
IFA29	2.83	$1.98 \times 10^9/cm^3$	$3.82 \times 10^7/cm^3$

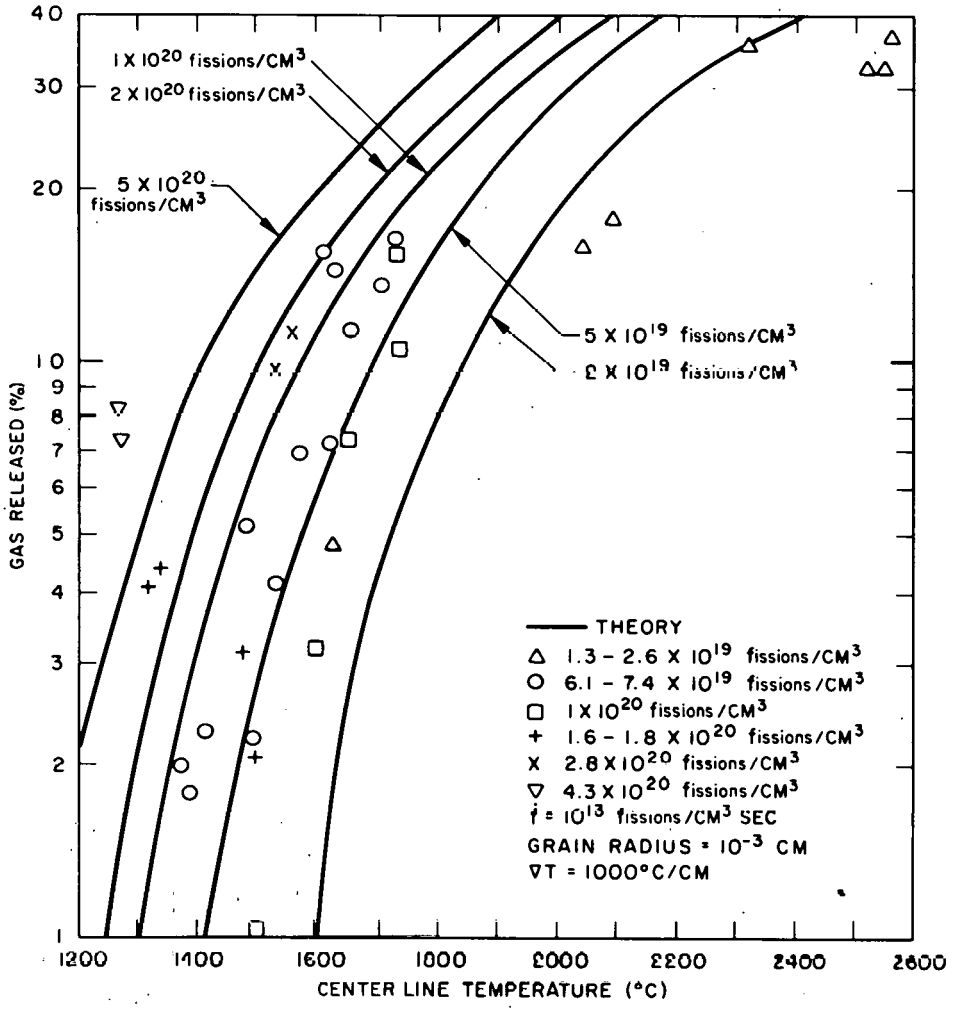

Figure 1. Comparisons Between Theory and Data of Lewis (Reference 20) for the Release of Gas in UO_2

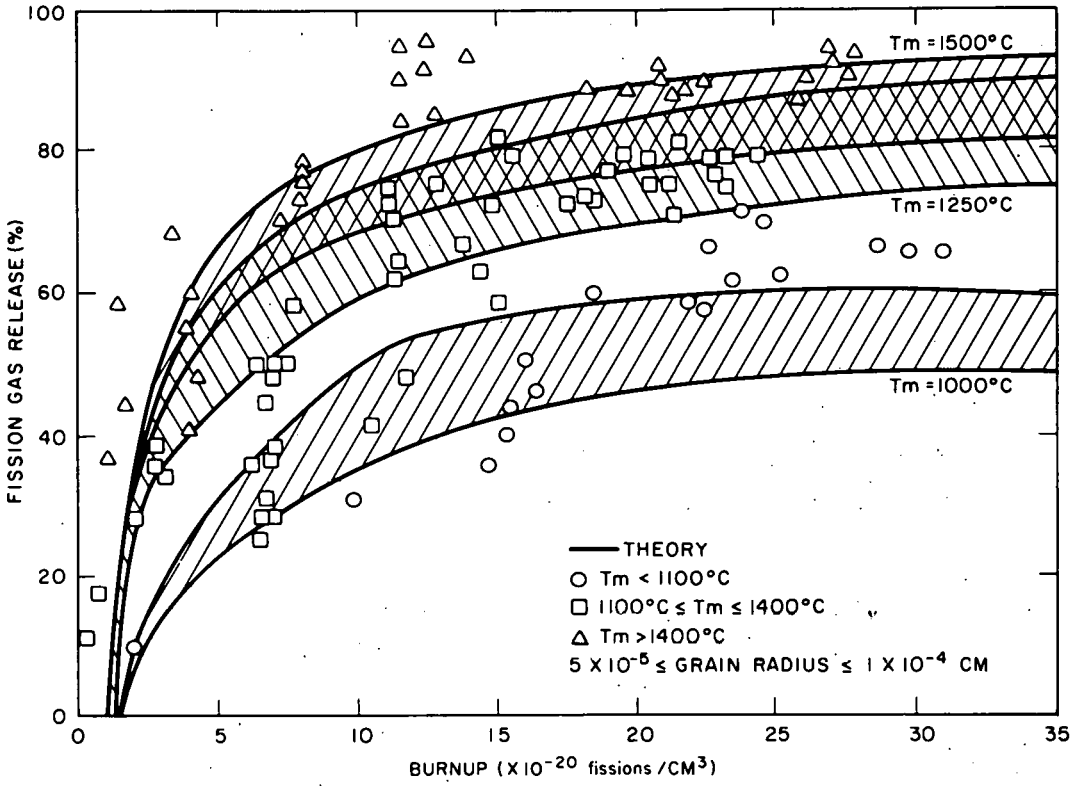

Figure 2. Comparisons Between Theory and Data of Zimmermann (Reference 21) for the Release of Gas in UO_2-20% PuO_2

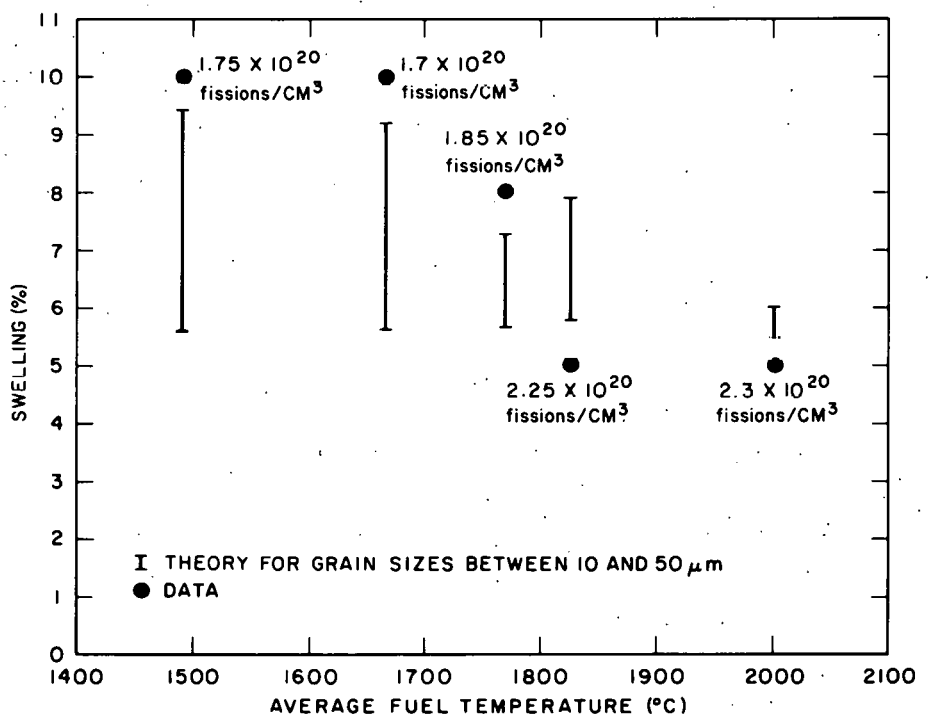

Figure 3. Comparison Between Theory and Data of Hilbert et al. (Reference 22) That Shows Swelling Versus Average Fuel Temperatures

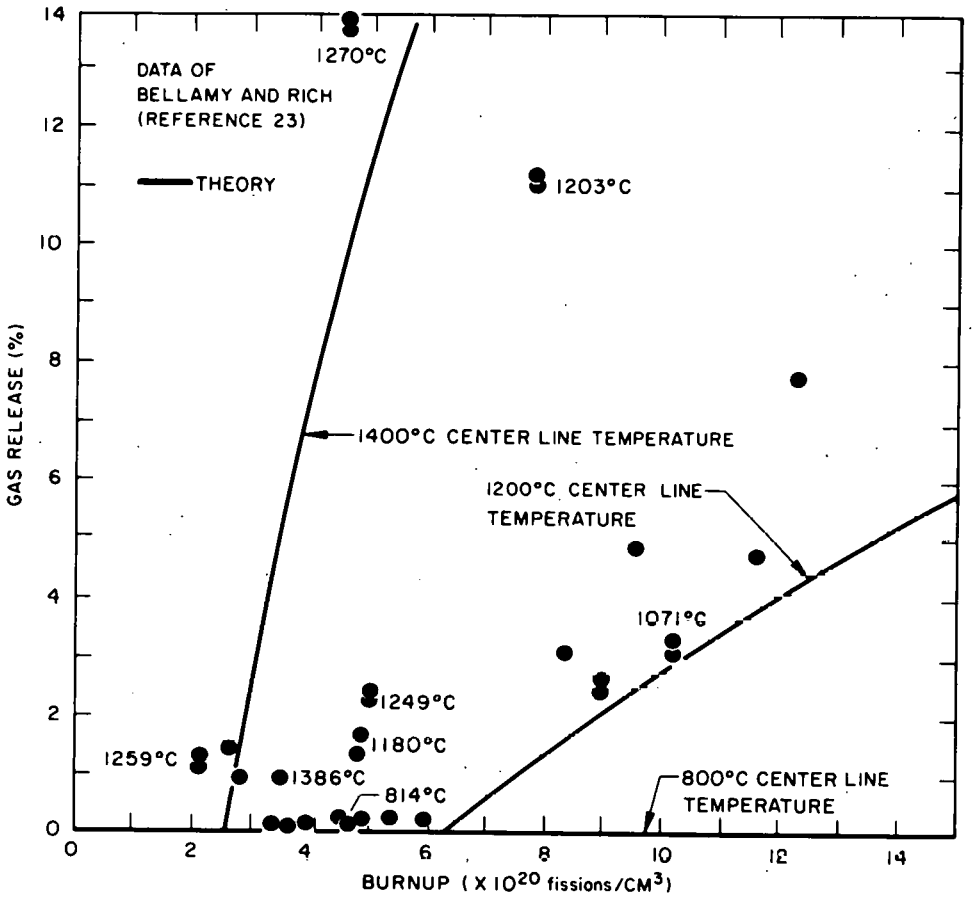

Figure 4. Gas Release Data of Bellamy and Rich (Reference 23) Versus Burnup

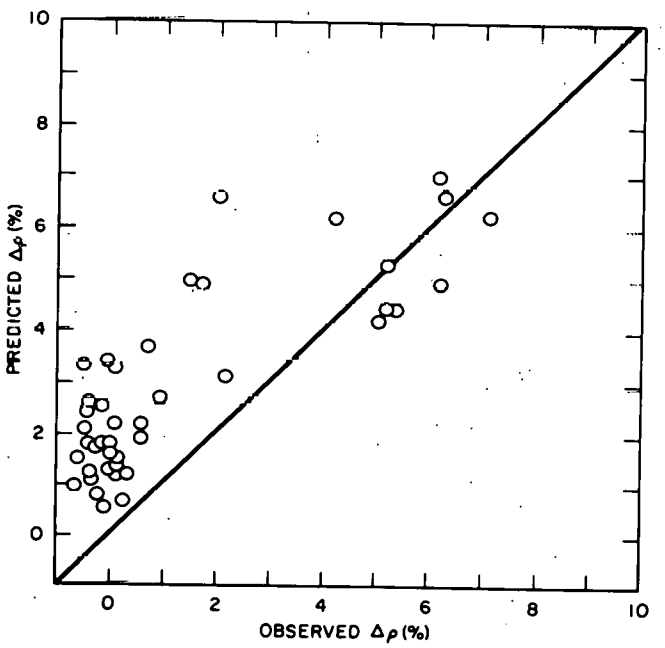

Figure 5. Comparison Between the Predicted and Observed Densification Data of Freshley et al. (Reference 24)

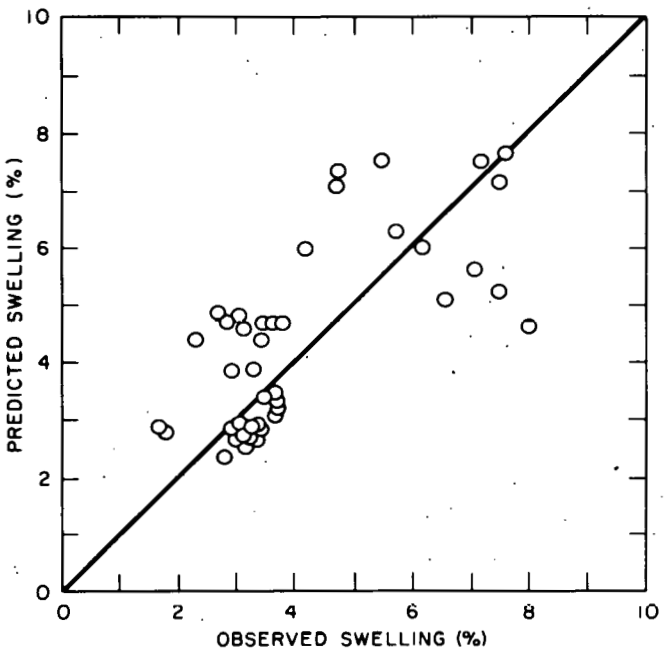

Figure 6. Comparison Between the Predicted and Observed Swelling Data of Banks (Reference 25)

*U.S. GOVERNMENT PRINTING OFFICE: 1978-703-115/658